The Pennsylvania State University

The Graduate School

Department of Meteorology

SPATIAL AND TEMPORAL EVOLUTION OF THE NOCTURNAL SURFACE LAYER

IN A SMALL, STEEP WATERSHED

A Thesis in

Meteorology

by

Burkely L. Twiest

Submitted in Partial Fulfillment
of the Requirements
for the Degree of

Master of Science

May 2014

The thesis of Burkely L. Twiest was reviewed and approved* by the following:

Kenneth J. Davis
Professor of Meteorology
Thesis Advisor

Scott Richardson
Research Associate

Marcelo Chamecki
Assistant Professor of Meteorology

Paul Markowski
Professor of Meteorology

Johannes Verlinde
Professor of Meteorology
Associate Head, Graduate Program in Meteorology

*Signatures are on file in the Graduate School

ABSTRACT

This study explores the conditions under which we can expect an early evening transition period (EET) to be established, and what measuring multiple terms of the surface layer energy budget can do to provide insight to the problem of the establishment and cessation of differential rates of cooling throughout a small valley. A network of temperature sensors, sonic anemometers, and net radiometers was deployed to the Shale Hills Critical Zone Observatory, a 0.08 km^2 forested valley in central Pennsylvania with a 49 m elevation change from valley bottom to ridge top. These sensors collected data during March-June 2013. Measurements were taken above-canopy (30 m above ground) and below-canopy (.91 m and 1.83 m above ground).

Study nights were separated to identify the EET period. Nights with an EET differed in several ways from non-EET nights; nights with an EET tended to have more negative average net radiation, calmer above-canopy wind speeds, and higher stability than non-EET nights. Three-month composites of these variables across the nighttime period of 1930-0600 LST show differences in temporal evolution throughout the night for net radiation, above-canopy wind speed, and air temperature decrease on EET vs. non-EET nights.

Ranking histograms indicated that both EET nights and non-EET nights showed spatial temperature patterns. The more variable spatial temperature pattern was found in the cluster with an EET, suggesting radiative sheltering does not fully explain the spatial temperature pattern on these nights. A primitive energy budget computed for three different case studies throughout the measurement period confirmed that many other terms were contributing to the valley cooling rate besides the radiative cooling. Horizontal advection and horizontal and vertical turbulent flux divergence both were of a larger magnitude than the radiative flux divergence on the EET nights.

No clear transition in the ABL, such as the development of down-valley drainage flow, was revealed to cause the change in the rate of cooling across the valley.

TABLE OF CONTENTS

LIST OF FIGURES

LIST OF TABLES

ACKNOWLEDGEMENTS

Chapter 1

Introduction

Meteorological phenomena occur on a wide variety of scales, across every terrain on Earth. Micrometeorology is the study of atmospheric processes occurring on a very small scale – typically less than 1km. The complexity of environments across the Earth allows for a wide variety of micrometeorological phenomena, from dust devils to turbulent eddies. This study focuses on the micrometeorology of the sub-canopy atmosphere within a small, forested valley.

1.1 Spatial Temperature Patterns in Complex Terrain with Vegetation

Mountain meteorology has a history of study dating back to the mid-nineteenth century, and knowledge of meteorological impacts of mountains was acknowledged as far back as 1648 with Florin Perier's mercury barometer measurements at the base and the summit of Puy de Dome in France (Barry 2008). Many studies of temperature have been undertaken in fairly large mountain ranges, such as Lundquist and Cayan's (2007) study of surface temperature patterns in the Sierra Nevada range of California or Tabony's (1985) study of minimum temperature in mountainous regions of Great Britain. Other studies have also characterized temperature patterns in gently sloped terrain, most notably the nocturnal cold air drainage phenomenon that can occur even at sites that are nearly flat (Bodine et al. 2009; Staebler and Fitzjarrald 2005; Mahrt et al. 2001).

Similarly, many studies have taken place in relatively flat, forested areas to understand the dynamics that a vegetative canopy adds to flow patterns (Froelich et al. 2011; Boldes et al. 2007; Finnigan 2000; Baldocchi and Meyers 1987). For example, Finnegan (2000) provides a

comprehensive description of turbulence in plant canopies. A majority of studies focus on the airflow within the canopy structure itself, but some are solely concerned with subcanopy motions.

Baldocchi and Meyers (1987) found evidence for a nocturnal change in the characteristics of the below-canopy space due to the increased stability dampening the turbulence beneath the canopy. They suggest that vertical and horizontal turbulence is not necessarily homogeneous beneath a canopy. Boldes et al. (2007) further supported the notion that the region near the ground of a dense forest is characterized by calmness relative to environments without vegetation. Shaw et al.'s (1990) study of pressure fluctuations took place both within and above a deciduous forest to connect pressure patterns within and below the canopy to the velocity field near the top of the canopy, and suggests that measurable differences in state variables such as pressure exist on extremely small scales. Subcanopy temperature is generally accepted as being roughly isothermal, at least during the leaf-on period (Sedlak et al. 2010), and therefore assumed to have no spatial pattern beneath the canopy in the absence of topography.

Other studies have combined vegetation and complex terrain in their investigation of spatial temperature patterns. Gustavsson et al. (1998) completed a transect of several valleys, some of them forested, and noted rapid cooling after sunset and the establishment of cold air pools. These cold air pools were much stronger in the forested regions of their transects. Belcher et al. (2008) reviews the dynamics of forested canopies in complex terrain, but again the emphasis is on the canopy and thus the trunk space is treated as roughly isothermal both horizontally and vertically. They also note the canopy's dampening of turbulence, allowing for more conducive conditions for drainage flows to form beneath the canopy.

Chen and Yi (2012) explore major controls of katabatic flows that include a vegetative layer via a theoretical model, and argue that katabatic flows reach a maximum speed because of drag force balancing the buoyancy force. This model explains why researchers have been divided as to whether steep or gentle slopes produce the highest velocity of katabatic flow. Steep slopes

increase gravitational acceleration of air, leading to a faster flow. However, the adiabatic compressional heating caused by rapid descent causes the buoyancy force to increase as well, suggesting that too steep of a slope is detrimental to rapid katabatic flows. They conclude that for strong vertical stable stratification, maximum katabatic flows form on gentle slopes, but under weakly stable stratification maximum katabatic flows occur on steep slopes.

Katabatic flows, otherwise known as drainage flows, are a type of buoyancy current that occur when a slope cools faster than its surrounding environment. This cooling creates an imbalance in the temperature field, which causes the cooler, denser air to flow downhill. Mahrt (1982) provides a theoretical description of the momentum balance of these gravity flows following from the momentum conservation equations. That work demonstrates several types of regimes that may be expected for different slope lengths, slope angles, and wind speeds. Drainage flows have been documented in all types and scales of sloping terrain, and the basic mechanisms of drainage flows have been known for decades (Vergeiner and Dreiseitl 1987; Mahrt 1982; Fleagle 1950). However, complexity of terrain and vegetation add to the complexity of drainage flows. Such flows can have complicated, three-dimensional structures, (Tóta et. al. 2012) and may play a role in the formation of below-canopy spatial temperature patterns.

1.2 The Early Evening Transition Period

A period of time known as the early evening transition period (EET) has been documented as the time when a spatial temperature gradient forms in a valley or other region of varied topography that will persist for the remainder of the night via rapid cooling (Acevedo and Fitzjarrald 2001). This temperature gradient formation has been noted by many groups, and a variety of mechanisms have been proposed to describe the formation of these gradients and their maintenance throughout the night. Figure 1-1 illustrates this phenomenon as captured by a

network of sensors in upstate New York in 1982 (Acevedo and Fitzjarrald 2001). It is clear that early in the night the rates of cooling differ at various stations, but that by later in the evening, a similar rate of cooling has been reached for all stations. Drainage flows may be critical in the formation of these local temperature gradients across complex terrain (Fleagle 1950).

One of the major theories behind the establishment of nocturnal spatial temperature differences in complex topography is differential radiational cooling (Karlsson 2000; Gustavsson et al. 1998). The timing of the cooling suggests that radiation is indeed a key component of the
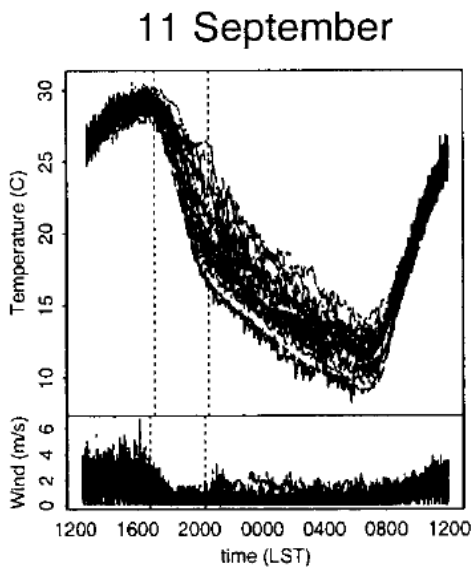
11 September

Figure 1-1. Adapted from Acevedo and Fitzjarrald 2001. The top plot shows the temporal evolution of temperature at each of their twenty-six stations for the night of 11 September 1982. The bottom plot shows the wind gusts at each station throughout the night.

cooling, but other factors may be involved in establishing these temperature gradients. The time evolution of the rate of change of temperature suggests that there is another mechanism at work than radiational cooling or radiational sheltering due to the differential rates of cooling throughout the night. While Acevedo and Fitzjarrald's 2001 study qualitatively identifies this period, it does not provide mechanisms behind the formation of the pattern or this evolution in cooling rate throughout the night.

The topographic radiational sheltering mechanism is suggested by other studies as the cause of the temperature differential across valleys observed by Acevedo and Fitzjarrald (2001). Karlsson (2000) puts forward that vegetative canopies provide a sheltering effect from both turbulence and background flow, which allows for the effects of radiational cooling to be more concentrated on near-surface temperatures. Vegetative canopies also can act as a barrier, allowing an easier decoupling from the above-canopy atmosphere. Gustavsson et al. (1998) made a rough theoretical calculation for the volume of air required to fill a cold pool observed in a 770m x 50m x 30m valley, and found that cold air formed from radiationally cooled slopes surrounding the valley that was advected into the cold pool by drainage flow could not have provided all of the air within the cold pool. They also noted larger temperature decreases within forested areas of their transects, suggesting that the canopy's wind sheltering effect is more important than its effect as a heat source. Together, these pieces of evidence suggest that wind and topographic sheltering do play a substantial role in the establishment of cold pools in localized pockets of low elevation by explaining some of the differential cooling rates.

However, neither radiative nor wind sheltering does not explain what causes the cessation of different rates of cooling at individual points in complex terrain. After a spatial temperature pattern is established in the EET, the pattern established remains remarkably consistent (Acevedo and Fitzjarrald 2001; Helmis and Papadopoulos 1996). Temperature networks show a rate of cooling that is similar at all sites throughout these valleys at various elevations above the valley floor once the EET is over. Since the sheltering elements such as vegetation and slope tend to be physical features that do not change throughout the night, some other mechanism must be occurring to cause the rates of change across complex terrain to become similar for all parts of the valley.

Vosper and Brown (2008) numerically simulate the condition of rapidly decreasing temperature and the development of a spatial gradient followed by a uniform cooling of the

temperature array by reducing the turbulent heat flux within the sheltered valley. Their results demonstrated that sheltering is an important mechanism for producing pools of cold air in small valleys. They claim that vegetative and topographic sheltering is sufficient to produce near-surface potential temperatures several degrees colder than the background environment, because the most sheltered areas at the bottom of the valley will decouple from the background flow first. However, their simulation was two-dimensional and thus did not take into account the full topography of a valley and the potential for drainage at the valley outlet. The claim that valley flow is stagnant is an oversimplification, particularly in complex, three-dimensional topography. They also note the rapid cooling at the beginning of the simulation's EET, followed by a decrease in the rate of cooling. However, the mechanism by which the cooling rate evolved was beyond the scope of their study.

Acevedo and Fitzjarrald (2001) suggest that horizontal inhomogeneity in cooling rates control the spatial variations set up during the EET. They observed that different evenings where the valleys within their study period were decoupled from the background atmosphere had similar spatial patterns of surface temperatures; warm stations tended to always be warm, and cold stations tended to always be cold. This spatial pattern was linked to the local relative elevation, defined as the difference between the station height and the mean height in a 3x3km area centered on the station. Therefore, their study suggests that the difference in cooling rates is linked to local topographic features. However, it should be noted that their study encompassed a variety of similar valleys, with one sensor in each valley. Therefore, the differences they were seeing occurred on a scale of multiple valleys.

Drainage flows can cause turbulent mixing of the atmosphere above them due to shear induced by the flow of air downslope (Alekseychik et al. 2013). This study focuses on the establishment and maintenance of a spatial temperature pattern within Shale Hills as related to the EET, including whether or not this phenomenon is closely related to the establishment of

drainage flows. The period of establishment for the temperature pattern, when different rates of cooling are occurring at different sites within the valley system, corresponds with the period of time where drainage flows are developing and maturing.

This study explores the conditions under which we can expect a spatial temperature pattern to be established, and what measuring multiple terms of the surface layer energy budget can do to provide insight to the problem of the establishment and cessation of differential rates of cooling throughout a valley. It is focused on a single valley, rather than spread across multiple valleys.

1.3 The Surface Layer Energy Balance Equation

The surface layer energy budget can be derived starting with the basic heat conservation equation (Stull 1988),

$$\frac{\partial \bar{\theta}}{\partial t} + \frac{\partial \theta'}{\partial t} + \bar{U}_J \frac{\partial \bar{\theta}}{\partial x_j} + \bar{U}_J \frac{\partial \theta'}{\partial x_j} + u_j' \frac{\partial \bar{\theta}}{\partial x_j} + u_j' \frac{\partial \theta'}{\partial x_j}$$

$$= \frac{\nu_\theta \partial^2 \bar{\theta}}{\partial x_j{}^2} + \frac{\nu_\theta \partial^2 \theta'}{\partial x_j{}^2} - \frac{1}{\bar{\rho} C_p} \frac{\partial \overline{Q_J{}^*}}{\partial x_j} - \frac{1}{\bar{\rho} C_p} \frac{\partial Q_j{}^{*\prime}}{\partial x_j} - \frac{L_v E}{\bar{\rho} C_p} \quad (1)$$

where θ is the potential temperature, U_j is the three-dimensional wind, x_j is the three-dimensional distance, ν_θ is the kinematic molecular viscosity, ρ is density of air, C_p is the specific heat of air, $Q_j{}^*$ is the three-dimensional net radiation, L_v is the latent heat of vaporization, and E is the evaporation rate. Terms with a bar over them represent average quantities, while terms with a prime are perturbations from the average. Following the reasoning of Stull (1988), we can Reynolds average and put the turbulent advection terms into flux form, giving

$$\frac{\partial \bar{\theta}}{\partial t} + \bar{U}_J \frac{\partial \bar{\theta}}{\partial x_j} = \frac{\nu_\theta \partial^2 \bar{\theta}}{\partial x_j{}^2} - \frac{1}{\bar{\rho} C_p} \frac{\partial \overline{Q_J{}^*}}{\partial x_j} - \frac{L_v E}{\bar{\rho} C_p} - \frac{\partial \overline{(u_j' \theta')}}{\partial x_j}. \quad (2)$$

where $u_j^{'}\theta'$ is the heat flux in three dimensions. The first term in this equation represents the mean

storage of heat, which is what we will be trying to predict and what we will independently

measure across the valley. The second term is the mean advection of heat by the mean wind. The

third term is the mean molecular conduction of heat, which is negligible. The fourth term is the

radiative flux divergence, the fifth term latent heat release, and the final term is the divergence of

the turbulent heat flux in three dimensions. Latent heat release is neglected in this budget since

the study is limited to the surface layer. However, direct measurements were obtained for the

advection, radiative flux divergence, and the turbulent flux divergences. This study also obtains

direct measurements of the change in surface layer air temperature over time to compare with

these terms in the energy budget. Effects of compression and expansion are accounted for by the

usage of θ. Only the vertical radiative flux divergence will be considered, using net radiometers

to measure incoming and outgoing radiation in the z direction above and below canopy.

Expanding (2) to show the coordinates explicitly and removing the thus far neglected terms yields

$$\frac{\partial\bar{\theta}}{\partial t} + \bar{u}\frac{\partial\bar{\theta}}{\partial x} + \bar{v}\frac{\partial\bar{\theta}}{\partial y} + \bar{w}\frac{\partial\bar{\theta}}{\partial z} = -\frac{1}{\bar{\rho}C_p}\frac{\partial\overline{Q_j^*}}{\partial z} - \frac{\partial\overline{(u'\theta')}}{\partial x} - \frac{\partial\overline{(v'\theta')}}{\partial y} - \frac{\partial\overline{(w'\theta')}}{\partial z}. \quad (3)$$

This is the equation our study measures and attempts to reconcile, determining how these terms

behave during the EET and their potential influence on the spatial temperature patterns seen in

the watershed on EET nights.

1.4 Spatial Scale of Prior Networks

A secondary goal of this study was to establish a network of temperature, radiation, and

wind measurements across a small watershed. Many networks tend to have stations tens or

hundreds of kilometers apart, and this spatial variation is often not sufficient to resolve small-

scale, terrain-induced micrometeorological features. Micronetworks have been established in

other locations (Bodine et al. 2009; Shapiro et al. 2009; Mahrt et al. 2001), and the data collected

by such networks provides a unique insight into spatial variations that may occur across tens to

hundreds of meters. Previously, many of the networks in the literature were placed in

topographically diverse areas, but areas that lacked vegetation (Tang 2006; Laughlin and Kalma

1990). Other studies have taken place in much larger spatial domains. Acevedo and Fitzjarrald's

(2001) study looked at a series of valleys and ridges across a kilometers-wide domain, with one

sensor at each valley studied. Because these measurements were taken at different locations

relative to the valley floor, they were able to discern the EET from a variety of valleys.

Gustavsson et. al (1998) traversed valleys that were hundreds of meters across at the valley floor.

The network in this study, located in moderate topography with a vegetative canopy, is much

smaller than what previous studies have examined and will provide new insights into the energy

balance and the early evening transition period across a small scale.

This study uses a very fine network to measure key characteristics of the early evening

transition period, identify environmental conditions associated with the EET, obtain direct

measurements of many terms in the surface layer energy balance, and explore the temporal and

spatial temperature patterns found throughout nights with an EET. Such a network has not yet

been utilized to examine the EET.

1.5 Goals of the Current Work

First, this study would like to explore if an EET can be observed across a single valley.

Acevedo and Fitzjarrald (2001) observed an EET across multiple valleys. No study has yet

observed this phenomenon across a single valley. If an EET is observed, this study will

characterize it further and contrast the characteristics of EET nights with those of non-EET

nights. The surface layer energy budget will be examined to determine which terms appear to

explain the rate of cooling seen within the valley, and whether the radiative flux divergence is the dominating term in this energy budget. Typical assumptions regarding the estimation of the radiative flux divergence will be compared to direct measurements of the turbulent flux terms to determine if they are appropriate. Finally, the surface layer energy budget will be compared between the regime of rapid cooling present during the EET and the less rapid, more steady cooling of the regime after the EET to determine if large differences between terms in the surface layer energy budget exist between these two regimes.

Chapter 2

Methods

This chapter presents an overview of the site, instrumentation and network layout, instrument calibration, and analyses performed on the data. Clustering algorithms, sorting of data into EET nights and non-EET, data selection criteria, filtering applied to the data and flux calculations are explained. Finally, the method of selection of case study days and quantification of the surface layer energy budget on those days are presented.

2.1 Site Description

The Susquehanna Shale Hills Critical Zone Observatory is a watershed located in the mountains of central Pennsylvania, at 40 39' 52.39" N, 77 54' 24.23" W and covers .08km^2. It is approximately 14.5km south-southeast of State College, Pennsylvania (Figure 2-1). The terrain of the region is characterized by ridges and valleys, similar to much of the Appalachian foothills. It is a forested watershed with a vernal stream that runs through the center of the valley during most of the year, except for the summer months. The valley is 49m deep, 450m long, and 240m across and oriented with the axis of the valley running nearly due west-east. The valley outlet is 256m above sea level. The entire watershed is densely forested. Near the valley outlet, the trees are mostly coniferous, approximately 75% eastern hemlock. As one progresses eastward and subsequently up the valley, the landscape quickly evolves into a deciduous forest with a few pines interspersed. Species in this mixed, largely deciduous forest include white oak, red oak, red maple, white pine, eastern hemlock, and cherry.
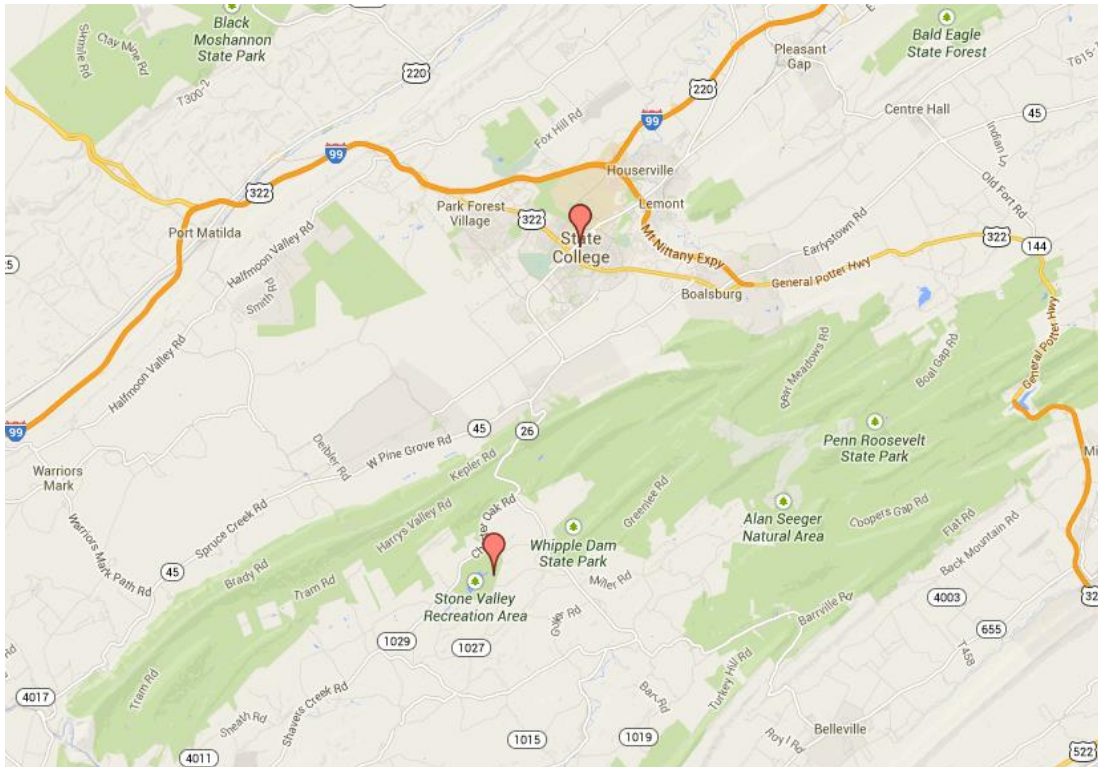
Figure 2-1. The location of Shale Hills Critical Zone Observatory relative to State College, Pennsylvania. (From maps.google.com)

The north and the south slopes exhibit different environmental characteristics. The north slope is south-facing, and thus receives more solar radiation than the south slope, which is north-facing. The south slope is also steeper, with an average slope of ~20° compared to a gentler, 15° average slope across the north slope. The understory on the south slope is mostly fallen leaves and branches, whereas the understory on the north slope is much more vegetated.

This study took place from March 28th, 2013 to June 24th, 2013. These dates were chosen to encompass leaf-on, leaf-off, and the transition between them. This time selection also avoided most of winter's snowfall, although a cold spring enabled snow to remain in the watershed at the start of the study. Mosses were present but not abundant during the entire study period, particularly on the north slope. A few plants sprouted on the south slope around mid-May and persisted until the end of the study in late June. This contrasted greatly with the understory on the north slope, which had more understory foliage throughout the entire study. At the beginning of May, more seasonal plants such as Mayapples (*Podophyllum peltatum*) began to sprout. These

plants covered the ground beneath the canopy and attracted several varieties of insects and
arachnids.

2.2 Instrumentation

Eleven instrumentation sites were established for the purpose of this experiment. The
data from these stations were used in conjunction with a 30m eddy covariance tower located at
the Shale Hills Critical Zone Observatory, denoted by the inverted blue triangle in Figure 2-2.
The eleven sites within Shale Hills are also illustrated in Figure 2-3. Four sites (two sites per
slope) were equipped with two HOBO data loggers and TMCx-HD water/soil temperature
sensors at .46m and .91m. One additional site on each slope was equipped with one HOBO
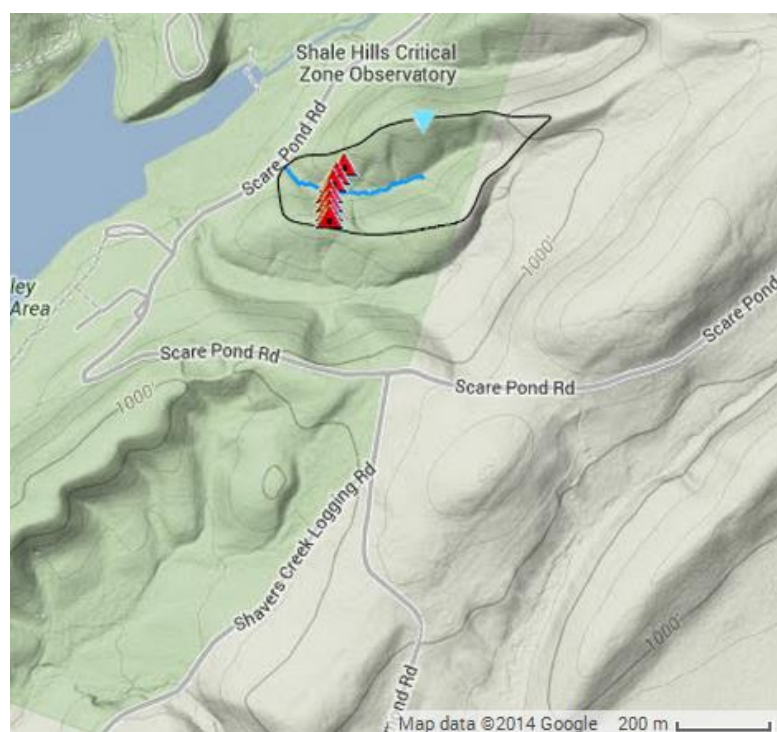
Figure 2-2. Topography at Shale Hills CZO. The red triangles mark the micrometeorology stations established for
the purpose of this study, and the inverted blue triangle is the location of the eddy covariance tower. The blue line
is the vernal stream located at the bottom of the watershed, and the black line marks the border of the Shale Hills
watershed.
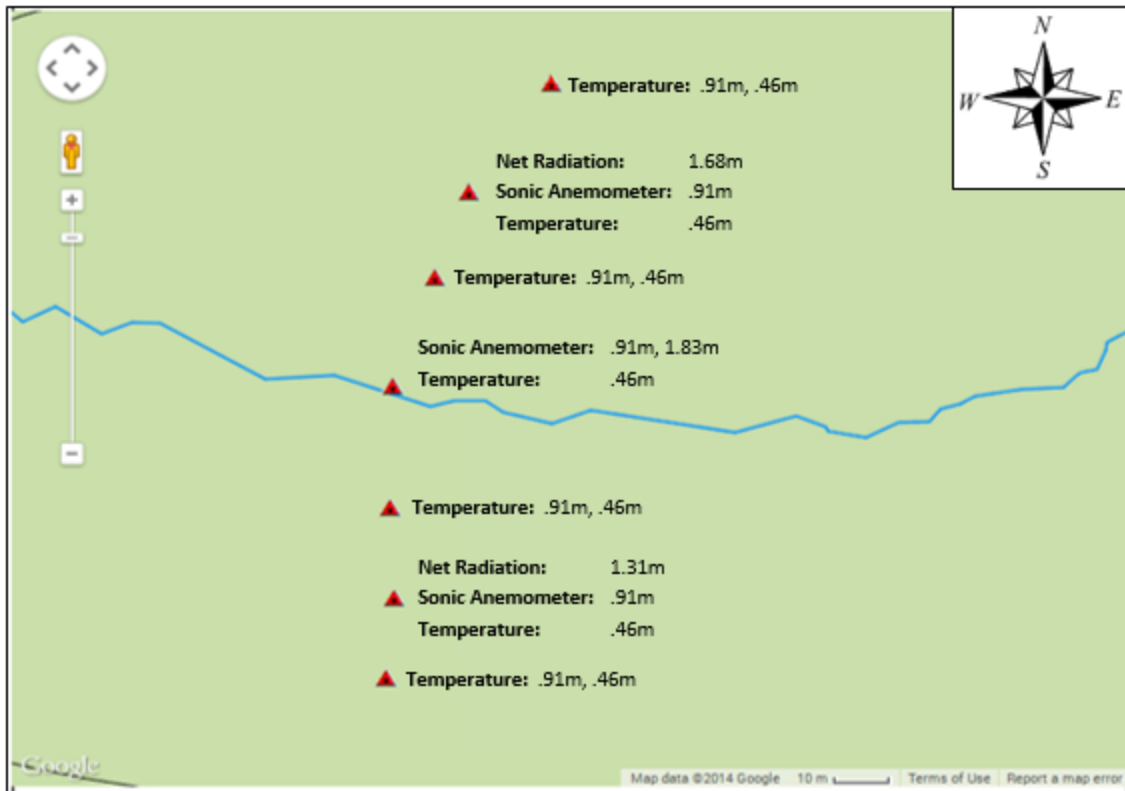
Figure 2-3. A description of the instrumentation at each station in the Shale Hills Micronetwork and their associated heights.

Figure 2-4. Three example instrument stations at Shale Hills. Instruments are circled in red (net radiometer), green (sonic anemometer), and purple (logger/temperature sensor). Stations pictured are representative of all surface measurement sites.

data logger and temperature sensor at .46m, a Campbell CSAT3 sonic anemometer at .91m, and a

net radiometer located at 1.31m on the south slope and 1.68m on the north slope. The final site

was located at the valley bottom, and consisted of one HOBO data logger and temperature sensor

at .46m and two Campbell CSAT3 sonic anemometers at .91m and 1.83m. Each of these types of

sites are pictured in Figure 2-4. The net radiometers at both slope sites were pointed due south.

The temperature probes were shielded by Styrofoam cups with air holes poked in them to ensure

sufficient airflow. The maximum elevation difference between stations in the network was 16m.

Figure 2-3 is a close-up of the micronetwork, with labels and elevation above the surface for each

sensor. Newer temperature sensors (NPro1, NPro2, and NPro3) have higher temporal resolution

than the other temperature sensors, and so were placed at the sites with the most extreme

elevations to capture the nuances of the ridge top and valley bottom temperature evolutions.

Above-canopy radiation measurements were taken at Rock Springs, a nearby research site

operated by the National Oceanic and Atmospheric Administration (NOAA) with assistance from

the Pennsylvania State University.

The watershed sonic anemometers were aligned with the valley axis in order to better

resolve downslope winds. Therefore, the coordinate system has the x (and therefore u) direction

aligned with the valley, and the y (v) direction aligned with the slopes. The anemometers

collected data at 10Hz throughout the period of the study. The above-canopy sonic anemometer

was aligned with the mean wind above the valley, and also recorded data at 10Hz. The

temperature measurements from the HOBO sensors were taken once per minute, as were the

radiation data both above-canopy and below-canopy. The data were downloaded manually from

memory card storage approximately once per week throughout the study period.

The sonic anemometers in the field were leveled relative to gravity and not aligned with

the slope. This alignment was used following the reasoning of Hammerle (2007), who studied the

difference between gravity-relative and slope-relative sonic anemometers regarding flow

distortion by the sonic anemometers. They concluded that flow distortion would occur in even the best case scenarios, and thus could not be helped by altering the alignment. Christen (2001) tested several sonic anemometers in the trunk space of a forest, and found the CSAT3 to satisfy

Sonic	1 Hz			10 Hz		
	U_x Offset (m/s)	U_y Offset (m/s)	U_z Offset (m/s)	U_x Offset (m/s)	U_y Offset (m/s)	U_z Offset (m/s)
PSU0378	**-.045**	.020	-.004	**-.045**	.025	-.007
PSU0368	-.055	.010	**-.037**	-.060	.012	**-.037**
PSU0376	**-.084**	-.042	**.023**	**-.084**	-.044	**.023**
PSU0374	**.070**	**-.020**	**.020**	**.070**	**-.020**	**.020**

Table 1. Sonic anemometer offset experiment results of trials run at 1Hz and 10Hz. Matching results for 1Hz and 10Hz are bolded.

requirements of below-canopy studies. Also, the differing slopes of the two valley walls change as one ascends or descends the valley walls, and it would be difficult to select an exact slope angle with which to align each sonic. Gravity remains a constant at all locations throughout the valley, and thus is a better standard of measurement in this case.

The sonic anemometers were tested for offset before deployment, to quantify the accuracy to which the wind measurements were going to be accurate within the range of wind speeds we expected to measure in the field. The "garbage bag" test recommended from the CSAT3 instruction manual was used; a garbage bag was taped over the sonic anemometer and measurements were taken for ten minutes in a still room to create an environment with zero wind speed. This test was run for two measurement rates: 1Hz and 10Hz. Errors for each sonic

anemometer are shown in Table 1. Good consistency is seen between the two experimental runs at different measurement frequency. These offsets were determined to not be large enough to affect our measurements extensively, as for U_x and U_y they are an order of magnitude smaller than the wind speeds observed described in the literature (Acevedo and Fitzjarrald 2001; Gustavsson 1995; Haiden and Whiteman 2005; Hammerle et. al 2007). U_z is typically smaller in magnitude than U_y and U_x, and thus results in the U_z direction have larger potential for error than results in the U_x and U_y directions.

The HOBO dataloggers and temperature sensors were tested for offsets both before and after the deployment. All of the sensors were run concurrently at three different temperatures. The sensors were shielded by Styrofoam cups to simulate actual deployment conditions. The array average was taken to be the true, reference temperature against which each sensor's offset was calculated via a three-point linear fit. The three points encompassed the typical range of temperatures the sensors experienced at Shale Hills and were measured at ambient air temperature, a typical refrigerator temperature, and a typical freezer temperature. Since the focus of our study is the differences in temperatures across the network and not the absolute temperatures, the average works well as the reference temperature. One of the HOBO dataloggers malfunctioned during the deployment and was replaced. Due to sensor representation issues that this malfunction raised, the post-deployment calibrations were used for the analyses, as the sensors used in post-deployment calibration were used throughout most of the study. However, the difference in the pre-deployment and post-deployment fit equations is quite small (aproximately 10^{-1}K) for all of the HOBO stations, even though the malfunctioning sensor was used in the pre-deployment fit and excluded in the post-deployment fit. Temperatures experienced throughout study range from about -8°C to 32°C, and the range narrows to -8°C to 20°C when considering only nighttime, according to records taken at the nearby University Park

airport, KUNV. At these temperatures, the temperature sensors are accurate within ±.25K

according to the manufacturer.

2.3 Analyses

2.3.1 Data Selection Criteria

The 10Hz data were compiled into thirty-minute averages for many of the analyses.

These averages were only computed if greater than 90% of the data was present for the thirty

minutes. Possible reasons for missing data include battery failure, memory card corruption, fog

formation, precipitation, or insect interference. The temperature sensors and dataloggers were

highly reliable throughout the study, and data for all days in the study were obtained. When

examining the net radiation data, negative spikes (net energy lost to the atmosphere from the

surface) were seen with values much below -500W/m^2. These radiation data were considered to

be faulty since they occurred singularly and were extreme values, and were excluded from the

analyses. Because the main phenomena studied is nocturnal spatial temperature patterns and

nocturnal drainage flows, only data collected between 1930LST and 600LST were used for

composites, and nights were named according to the date on which they started.

2.3.2 Weka Clustering and Cluster Comparison Methods

Weka version 3.6.8 (Hall et. al 2009) supplied the algorithms used for sorting and

classifying the environmental data collected. Fifteen variables were included for analysis. Some

of these variables had numeric values: the night start date, average above-canopy net radiation,

average above-canopy wind speed, average south slope wind speed, average north slope wind

speed, average valley bottom wind speed, spatial pattern strength, temperature difference between

the north slope and the valley bottom, temperature difference between the south slope and the

valley bottom, valley bottom vertical temperature difference, and temperature difference between

the tower and the valley bottom. Other variables were categorical. Presence of downvalley flow

(parallel to the sonic anemometer alignment) and presence of downslope flow (perpendicular to

the sonic anemometer alignment) were assigned a value of zero if the flow in question was

absent, one if it was present at some stations but not all (such as if we had downslope flow on

only one slope), and two if it was unquestionably present at all stations. The above-canopy wind

direction was also parameterized by three numbers – zero represented cross-valley (north-south)

flow at the tower, two represented along-valley (east-west) flow at the tower, and one represented

oscillating or mixed wind directions prevailing for most of the night. Presence of downvalley

flow, downslope flow, and above-canopy wind direction were visually identified by wind
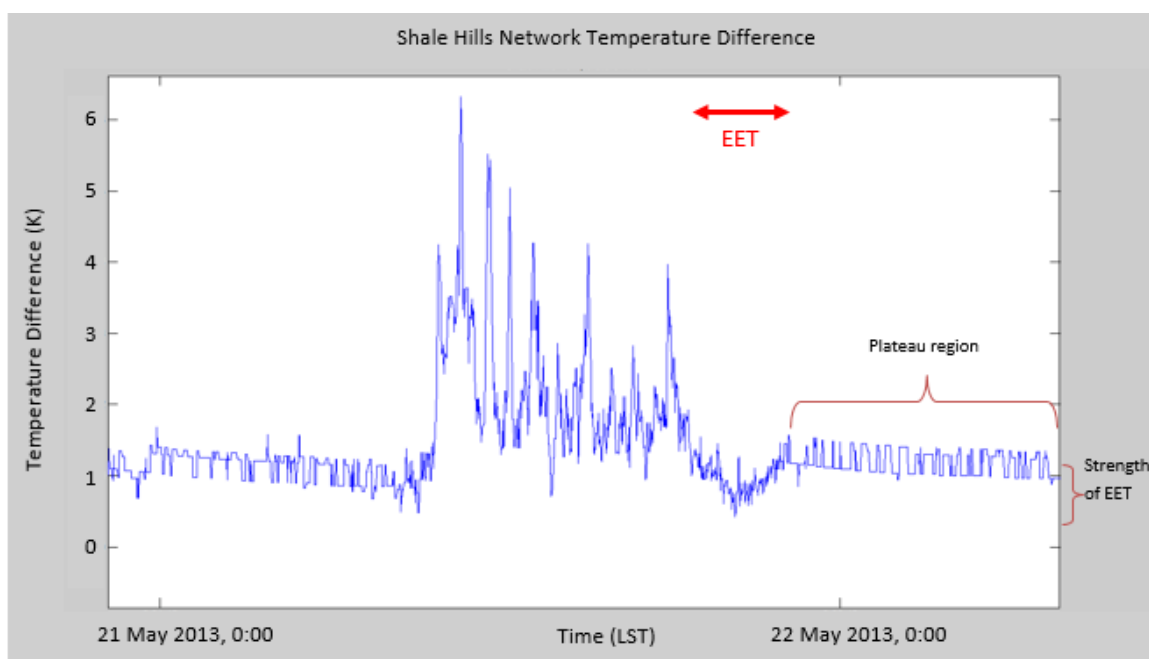
Figure 2-5. An illustration of how the strength of the EET was calculated from a sample night (May 21-22, 2013). The difference between the absolute warmest and absolute coldest temperature in the micronetwork is on the y-axis, and the time is on the x-axis. The red arrow corresponds to the EET period.

direction shifts that persisted at the relevant sonic anemometers. Finally, canopy presence was

parameterized in a binary fashion – the value of this variable was zero if the leaves in the valley

had already emerged and one if the valley was leafless. There is no leaf transition period

represented in the canopy variable; the date of May tenth was chosen as a cutoff based on several

photographs taken throughout the study period.

The strength of the EET was determined to provide better correlation with the other

variables than a binary variable indicating whether or not an EET occurred. For this reason, the

strength of the pattern was used in the analyses instead of merely the presence or absence of the

EET pattern in the temperature traces. The strength of the early evening transition was

determined by plotting twenty-minute averages of the maximum difference between the sensor

with the highest temperature and the sensor with the lowest temperature. These sensors were

allowed to change with time; the absolute maximum and minimum temperature across the entire

network for each ten-minute average were used in this calculation regardless of sensor location

within the network. A local minimum followed by a plateau was observed on nights where a

temporal temperature pattern was visually observed across the network – EET nights. The value

used to represent the strength of the pattern is calculated by subtracting the local minimum after

sunset from the average plateau value of the difference between the highest and lowest

temperature across the network. A value of zero was assigned if no local minimum was present.

Figure 2-5 illustrates key elements of the EET strength variable. The HOBO temperature sensor

at the valley bottom was excluded from the difference in maximum and minimum temperature, as

its large topographic and radiative sheltering consistently resulted in a much different temperature

(up to 2-3K) than other sensors in the micronetwork, even those only a few meters away. This

difference between the valley bottom sensor and the other sensors did not differ between EET and

non-EET nights, and so it was determined that the lowest temperature sensor would be excluded

only from determining the strength of the spatial temperature pattern. It is included in all other analyses.

The search method BestFirst was combined with the attribute evaluator CfsSubsetEval to determine which variables were best able to predict the strength of the EET pattern. The combination of the BestFirst algorithm and the CfsSubsetEval algorithm evaluates the worth of a subset of attributes by considering the predictive ability of each feature and the degree of redundancy between the variables. Therefore, if attributes are closely correlated to one another, the one that has the stronger ability to predict EET formation will be selected. Through these algorithms, a subset of features that are highly correlated to EET formation while not being highly intercorrelated with each other is created.

Two clusters were then formed using the k-means clustering algorithm with the previously selected variables to determine the relative significance of each factor with regards to the EET strength. While the previous algorithm selected which variables were important to the EET formation, this algorithm sorts the nights based on those important variables. The k-means clustering algorithm partitions *n* observations (in our case 88) into *k* sets (in our case 2). Each observation belongs to the cluster with the closest mean to the observation being clustered around. These two groupings of nights will be compared to examine differences between EET nights and non-EET nights.

A ranking analysis was also performed for each type of night, using both rank histograms and composite ranking evolution. To perform the ranking analysis, the HOBO temperature sensors were given a label of 1-11, with 1 being the warmest temperature sensor in the micronetwork and 11 being the coldest temperature sensor in the micronetwork. Nights were separated into EET nights and non-EET nights, and the rankings were analyzed in two ways. Composite evolutions gave a sense of how the pattern evolves throughout the night or remains steady, and whether the sensor's location or other factors have a greater effect on the temperature.

If the sensor's location were the largest influencing factor on the ranking of the temperature sensor relative to all of the other sensors, we would expect consistent rankings on EET nights throughout the night.

For this composite evolution analysis, the rankings were assigned for every ten-minute period throughout the course of the night, resulting in sixty-three periods of ranking per night. Histograms of rank occurrence were also created, but the histograms were based on the rank of the sensor for the temperature averaged across the entire night. This analysis highlights the temperature pattern differences between the types of nights for each individual temperature sensor and demonstrate how similar nights within each cluster are to each other. The more similar nights within a particular cluster are, the sharper the peak that will be seen in that temperature sensor's histogram.

2.3.3 Flux Calculation and Energy Budget Development

Fluxes were among the values computed at half-hour intervals for each sonic anemometer within the network, enabling the calculation of horizontal flux divergences in the slopewise direction and vertical flux divergences on the valley bottom. When calculating the terms in the surface layer energy balance, three pairs of case studies were considered. These pairs consisted of an EET night and a non-EET night only one or two nights apart. By ensuring that the dates were located close together in time, potential inter-seasonal variability was limited as much as possible. One pair of dates was taken from the beginning of the study – March 29th (an EET night) and March 31st (a non-EET night) and one pair of nights was taken from the end of the study period – June 8th (EET) and 6th (non-EET). In both of these cases, the non-EET night was identified by the lack of temperature variation throughout the night, which corresponds to a plateaued difference in network temperature differential variability: the opposite of what is occurring in Figure 2-5.

There was also no obvious evolution of the temperature at one sensor with regards to the other sensors in the network on these non-EET nights. The differences between sensors remained uniform. Temperature dropped only a couple degrees Celsius on both of these non-EET nights. The choice of these distinct non-EET nights allowed for analysis of the difference in terms that support EET nights versus those supporting nights that show no evidence of EET.

The pair of dates in May was chosen as a different type of case study. For this pair of dates, the EET night was easily selected, but the non-EET night that was chosen showed some time periods of cooling that looked like the beginning of an EET. The selection of this night as a non-EET night was to shed light on what prevents nights from fully undergoing EET, even if they initially show a temperature drop or show an EET-like temperature drop at some point during the night.

Pairs of EET nights and non-EET nights were compared for differences in the various terms of the surface layer energy budget, as well as specific values of environmental variables like the radiative flux divergence. A height of 30m was estimated for the depth of the radiative flux divergence due to the decoupling of the valley layer from the 30m tower on EET nights. The canopy aided in this decoupling once it emerged in mid-May.

Flux divergences in the valley-wise direction were neglected for the budget calculations due to the setup of the instrument array. This network was set up to sample the anticipated direction of the flow, which was primarily anticipated to be on the slopes rather than along the less steeply-angled valley axis. The two dimensionality of the array prevents measurement of the horizontal flux *divergence* in the valley-wise direction, though the horizontal flux at each site was calculated in both the slope-wise and valley-wise direction.

Energy budgets were calculated for the entire night on each of our EET nights, as well as for each of the two regimes seen on EET nights: the EET period and the second, calmer regime where temperatures continue to decrease, but a spatial temperature pattern has been established

that persists after the EET cooling period. This budget calculation was achieved by averaging the energy budgets calculated at each half hour. Plots were then made of each component of the budget, to determine which measured terms had the largest impact on the budget as a whole. When measuring the horizontal flux divergence, the flux divergence was calculated between the south slope (sonic anemometer at 1.5m) and the valley bottom sonic anemometer at 1.5m. These two sites were chosen as the basis for the horizontal flux divergence calculation because they are at the same elevation above ground, and successfully collected data on selected case study days.

Chapter 3

Results and Analysis

This chapter will describe the results of the clustering of the nights into Early Evening Transition (EET) and non-EET nights. Then it will explore what characteristics describe the EET and non-EET nights, and what makes them different. It will go on to describe the spatial temperature patterns on EET and non-EET nights. Finally, the sub-canopy energy balance will be contrasted for EET vs. non-EET nights. The budget will be examined for what terms are important and if the budget can be brought to closure with what this experiment measured.

3.1 Clustering Results

Weka's k-means algorithm sorted the eighty-eight nights in our study into two clusters, approximately broken down by presence or lack of an EET as described in Chapter 2. Two clusters were found to be the most effective in sorting between EET and non-EET nights with regards to spatial temperature patterns. While three clusters was also attempted, strong differences between weak EET nights and strong EET nights were difficult to distinguish. Thus, two clusters were used rather than three.

Due to the number of variables in the Weka dataset and their interactions, there were a few nights in the EET cluster that did not visually appear to have a strong EET (i.e. no evening local minimum was visually identifiable in the difference between the minimum and maximum temperature in the network), and vice versa. Nonetheless, these clusters were maintained as is throughout the analysis. The complete list of variables considered in the BestFirst and CfsSubsetEval search and classify algorithms is found in Table 2, along with whether or not

Attribute	Selected by BestFirst+CfsSubsetEval
Strength of EET	Variable being Predicted
Net Radiation	Yes
Night Start Date	Yes
South Slope Wind Speed	No
North Slope Wind Speed	Yes
Valley Bottom Wind Speed	No
N. Slope-Valley Bottom ΔT	Yes
S. Slope-Valley Bottom ΔT	No
Valley Bottom Vertical ΔT	No
Above Canopy-Valley Bottom ΔT	Yes
Presence of Downvalley Flow	Yes
Presence of Downslope Flow	No
Above Canopy Wind Direction	Yes
Above Canopy Wind Speed	Yes
Canopy Presence	No

Table 2. All variables fed into Weka's BestFirst + CfsSubsetEval algorithms to determine which variables were significant in predicting the strength of the EET.

the BestFirst and CfsSubsetEval algorithms considered them significant to a EET formation.

Previous studies have only considered the temperature decrease, decay in wind gusts, and specific

humidity jumps as the variables important to characterizing an EET (Acevedo and Fitzjarrald

2001), but this study finds several other variables that are closely linked to the EET.

Eight variables were found to be important in determining whether or not a spatial

temperature pattern would form. Forty-one nights were in the cluster containing EET nights, and

forty-seven nights were in the cluster containing non-EET nights. Interesting differences arise

between the two clusters. The calendar of which nights are EET and non-EET is displayed in

Figure 3-1. Both EET nights and non-EET nights typically occur on multiple nights in a row.

EET nights tend to occur earlier in the study period than non-EET nights, as exhibited by the

earlier average date of occurrence of EET nights. More transition nights were observed in the

colder, winter-like part of the study before leaves had emerged on the trees. The average net

radiation was also approximately 20W/m^2 more negative on EET nights, indicating that these

nights were subject to greater radiative cooling. The average above-canopy wind speed was lower

on transition nights than non-transition nights. Below canopy, the wind speeds are even smaller

and no significant conclusions can be drawn from the north slope winds about differences

between EET nights and non-EET nights due to the small difference in north slope wind speeds.

The downvalley flow variable shows a considerable difference between clusters. Recall

that a value of zero specifies that no downvalley flow was present, a value of one specifies that at

Attribute	All Data (88)	EET Nights (41)	Non-EET Nights (47)
Strength of EET (K)	.1957	.2504	.1480
Start Date (day of year)	130.5	125.37	134.98
Net Radiation (W/m^2)	-40.57	-50.42	-31.97
Above-Canopy Wind Speed (m/s)	1.79	1.67	1.90
North Slope Wind Speed (m/s)	.31	.32	.31
Downvalley Flow (dimensionless)	.909	1.769	.159
Above-Canopy Wind Direction (dimensionless)	1.28	1.46	1.13
N. Slope – Valley Bottom Δθ (K)	.175	.090	.250
Tower – Valley Bottom Δθ (K)	4.26	4.54	4.00

Table 3. Cluster comparison of relevant environmental variables. The EET night cluster consists primarily of nights that did develop an early evening transition period. The non-EET cluster consists primarily of nights without a transition. Values reported are the means over all of the nights contained within that cluster or over the entire study period.

least one station showed signs of a downvalley flow, and that a value of two specifies that downvalley drainage flow is occurring across all sonic anemometers within the valley. For the transition nights, downvalley flow was occurring at one or more sonic anemometers for a vast majority of the nights, whereas for the non-transition nights, downvalley flow was much less common.

The two temperature difference variables, which are measures of stability, also show differences between the clusters. The north slope-valley bottom measurements on average show a

March 2013						
Sunday	Monday	Tuesday	Wednesday	Thursday	Friday	Saturday
				28	29	30
31						

April 2013						
Sunday	Monday	Tuesday	Wednesday	Thursday	Friday	Saturday
	1	2	3	4	5	6
7	8	9	10	11	12	13
14	15	16	17	18	19	20
21	22	23	24	25	26	27
28	29	30				

May 2013						
Sunday	Monday	Tuesday	Wednesday	Thursday	Friday	Saturday
			1	2	3	4
5	6	7	8	9	10	11
12	13	14	15	16	17	18
19	20	21	22	23	24	25
26	27	28	29	30	31	

June 2013						
Sunday	Monday	Tuesday	Wednesday	Thursday	Friday	Saturday
						1
2	3	4	5	6	7	8
9	10	11	12	13	14	15
16	17	18	19	20	21	22
23	24					

EET   Non-EET

Figure 3-1. A calendar of all nights in the study. Blue nights are EET nights, and orange nights are non-EET nights.

difference of about .15K between transition nights and non-transition nights, with transition nights having less stable conditions. The tower-valley bottom temperature difference is larger for both clusters than the north slope-valley bottom measurements, as expected. The tower was regularly ~4K warmer than the valley bottom, and on nights with an early evening transition period the tower to valley bottom difference was about .5K larger, suggesting that the atmosphere was more stable during the transition nights than the non-transition nights.

The data-mining algorithms isolated the north slope as the important slope for discerning the formation of the spatial temperature pattern via the north slope wind speed and the north slope-valley bottom temperature difference, even though the north slope wind speed difference between clusters seemed to be within the range of error for the CSAT3 and therefore was not identified as significant on a practical level.

3.2 Within-Valley Conditions Associated with EET Observation

3.2.1 Temperature Decreases

The EET is illustrated in Figure 3-2; the spreading of the temperatures in the early evening transition period and following consistent cooling is what was identified both by Acevedo and Fitzjarrald (2001; see Figure 1-1) and by this study. Taking the temperature analysis one step further, when transition nights and non-transition nights were composited, large differences in the total amount of cooling occurs between EET nights and non-EET nights (Table 4). Transition nights show an average temperature drop within the valley of approximately 10K, whereas non-transition nights show an average temperature drop of 6K. Most of this rapid cooling occurs in the first few hours of the night, during the EET.
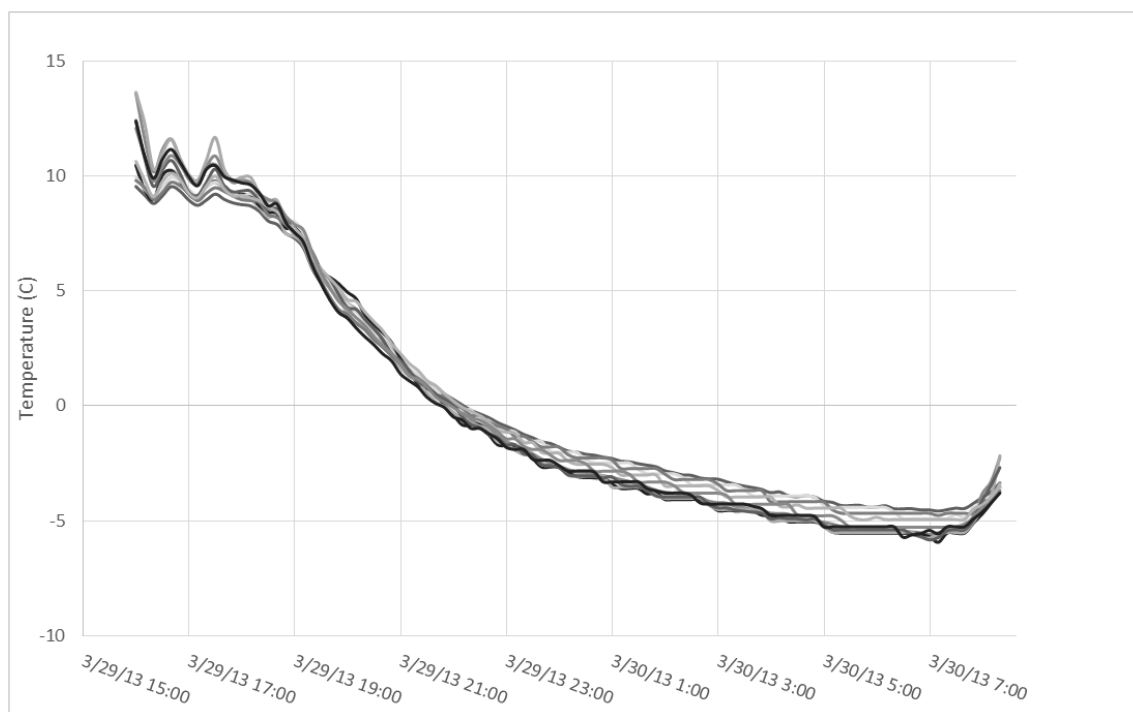
Figure 3-2. Early Evening Transition period observed on 29 March, 2013 across the Shale Hills watershed. Each line represents a different temperature sensor in the network. The time period of the plot (1930-0600 LST) is standard for the time period examined in all composite analyses.

On all nights, the valley is cooler than the tower, but some differences exist here between transition and non-transition nights as well. Both EET nights and non-EET nights begin with lower temperatures than the tower, and widen the temperature between the tower and the valley bottom match up well with the differences stated in Table 4, which are averaged across the entire night (1930-0530 LST).

	Tower-Valley Bottom ΔT, Start of Night (K)	Tower-Valley Bottom ΔT, End of Night (K)	Network ΔT Across Night (K)
EET	4	5	10
Non-EET	3	4	6

Table 4. Behavior of the network temperatures across the entire night (1930-0530LST) with respect to the tower and time. The valley bottom sensor referred to is the HOBO sensor located at .46m.
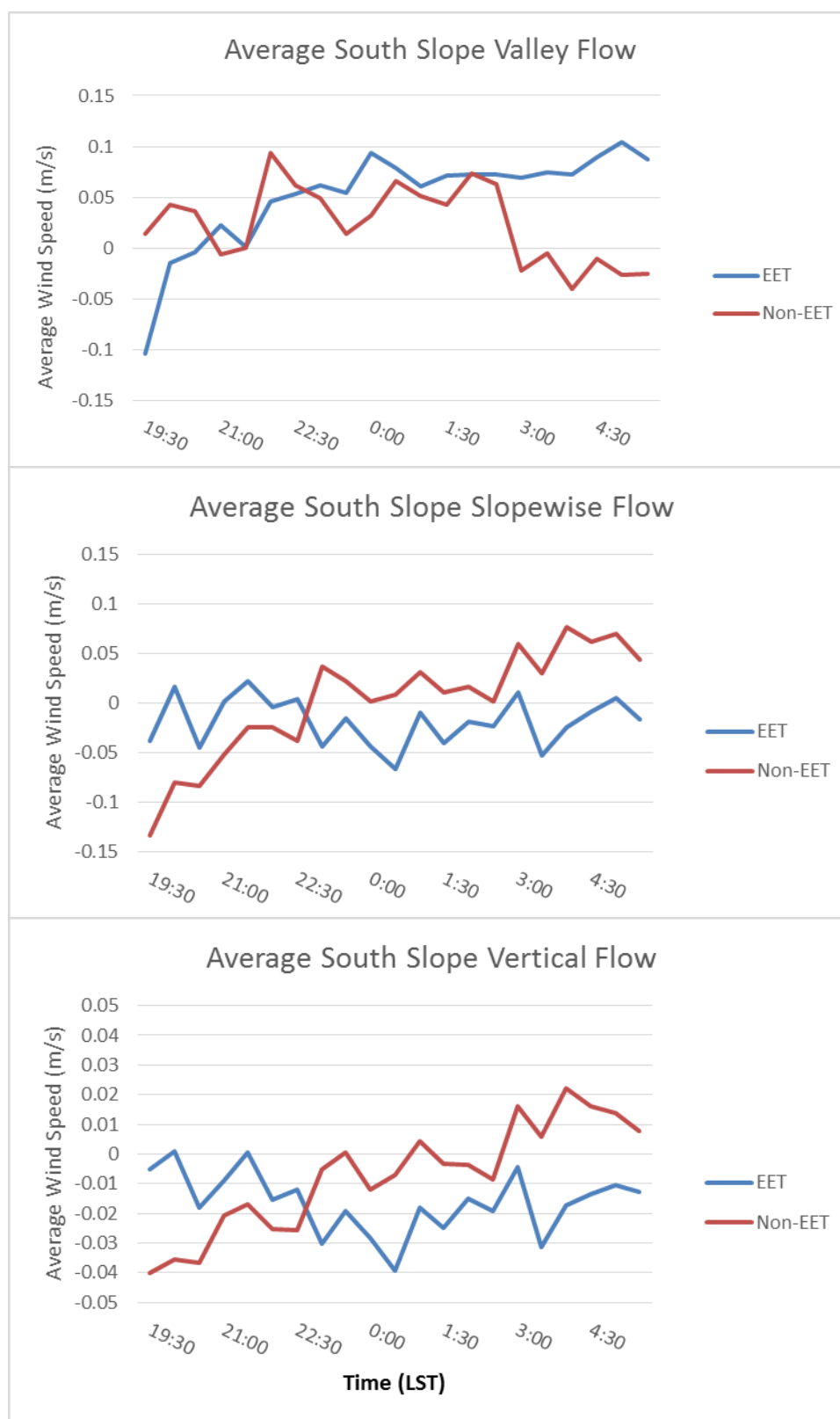
Figure 3-3. Composite wind speeds of all transition nights and non-transition nights on the south slope of the Shale Hills CZO. Positive valley flow corresponds to downvalley flow, negative valley flow corresponds to upvalley flow, positive slopewise flow corresponds to upslope flow, negative slopewise flow corresponds to downslope flow, positive vertical flow corresponds to upward flow, and negative vertical flow corresponds to downward flow.

3.2.2 Slope Winds

Wind measurements on each slope also showed differences between transition and non-transition nights, as well as differences between the slopes themselves. Figure 3-3 shows a composite of the south slope wind components for transition nights and non-transition nights. In this case, there are twenty-eight EET nights and twenty-seven non-EET nights in these composites. The sonic anemometers were oriented parallel to the valley axis, such that the positive valley-wise direction corresponds with downvalley winds and the positive slopewise flow corresponds with upslope winds. The anemometers were also oriented with respect to gravity, meaning that some of the upslope/downslope flow may be captured in the vertical direction.

Clear wind pattern differences developed in the valley on EET vs. non-EET nights. As these figures show, evidence of a downslope drainage flow on the south slope does not exist when transition nights and non-transition nights are composited. However, the composite plot of valley flow on transition nights shows a clear shift to downvalley winds fairly early in the night, which persists throughout the night. There is also a shift in the vertical flow tendency toward downward flow, which could be capturing part of the downvalley flow. Non-transition nights show relatively strong upslope flow developing toward the end of the night, as well as less-prominent upvalley flow in the early morning hours. Non-transition nights also show a positive trend in vertical flow, again capturing portions of the upslope and the upvalley flow.

The north slope wind data is similarly inconclusive as to the existence of a slopewise drainage flow (Figure 3-4), and the composites do not demonstrate a clear downvalley flow. The composites in Figure 3-4 encompass twenty-three EET nights and twenty-seven non-EET nights. The orientation of the sonic anemometer with regards to the valley and the slope is the same as the south slope anemometer, but in this case positive slopewise flow corresponds to downslope
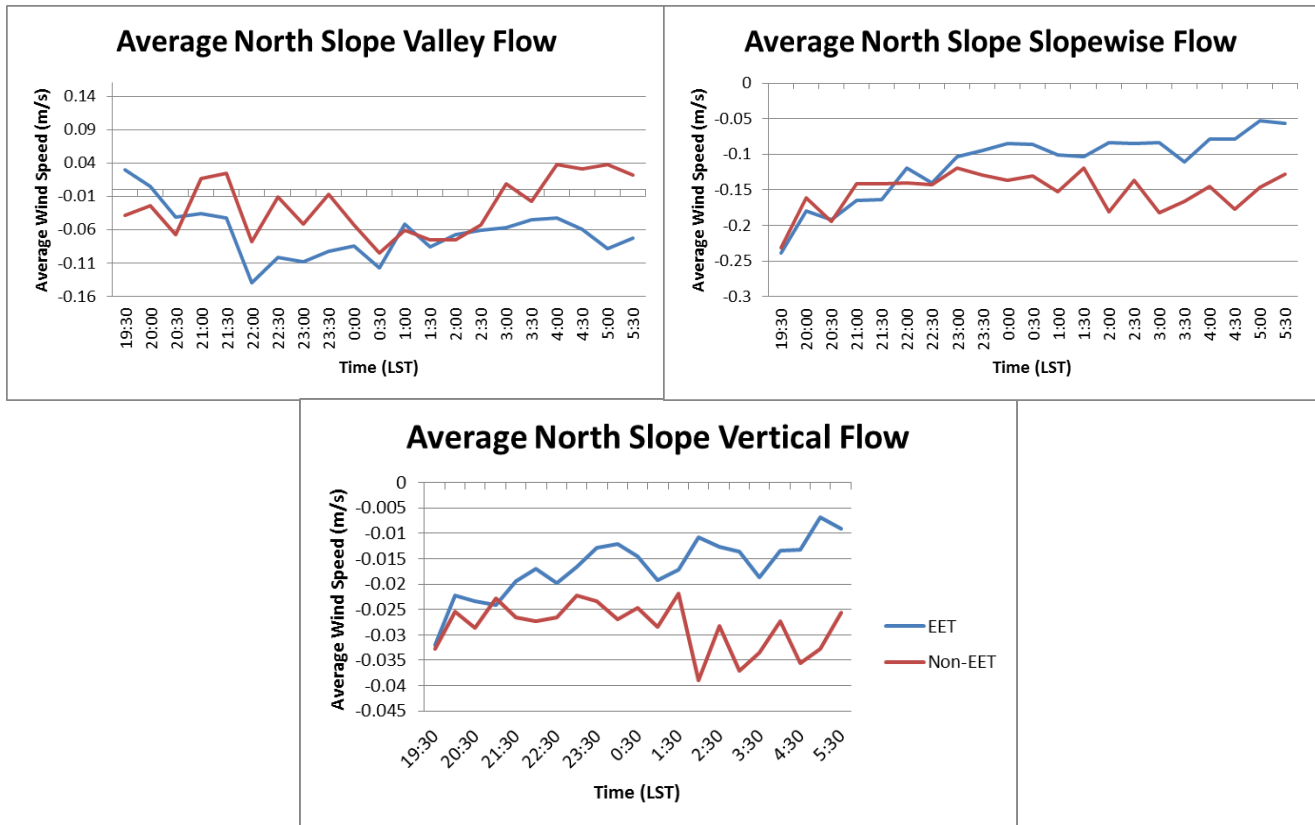
Figure 3-4. Composite wind speeds of all EET nights and non-EET nights on the north slope of the Shale Hills CZO. Positive valley flow corresponds to downvalley flow, negative valley flow corresponds to upvalley flow, positive slopewise flow corresponds to downslope flow, negative slopewise flow corresponds to upslope flow, positive vertical flow corresponds to upward flow, and negative vertical flow corresponds to downward flow.

flow and negative slopewise flow corresponds to upslope flow. The shallower north slope showed very weak evidence of upvalley flow during both transition and non-transition nights, though the flow was more steady on transition nights. There was a tendency toward upslope flow lessening across the night, which may have turned to downslope flow at the end of the night. This may be showing that a downslope flow is developing on this slope during transition nights. It is difficult to rely on the exact numbers since the flow is extremely weak, but the trend in the winds is away from upslope flow and toward downslope flow throughout the night does exist in these composites.

Two CSAT3 sonic anemometers were located at the valley bottom, at two different elevations above ground. Composite wind speeds for transition nights and non-transition nights for these anemometers are given in Figure 3-5. These two sonic anemometers show a definite shift toward downvalley flow at the start of the evening on transition nights, but not on non-EET

nights. These sonic anemometers show remarkably good agreement between them, providing further evidence that the flow detected is both existent and deep enough to be detected at both transition nights. This shift demonstrates the presence of a downvalley drainage flow on EET nights at .91m and 1.82m at the valley bottom. With additional consideration of the south slope anemometer, three sonic anemometers are showing evidence for a downvalley flow on EET nights.

Figure 3-5. Composite wind speeds of all EET nights and non-EET nights at the valley bottom of the Shale Hills CZO at two different heights above ground. Positive valley flow corresponds to upvalley flow, negative valley flow corresponds to downvalley flow, positive slopewise flow corresponds to northerly flow, negative slopewise flow corresponds to southerly flow, positive vertical flow corresponds to upward flow, and negative vertical flow corresponds to downward flow.
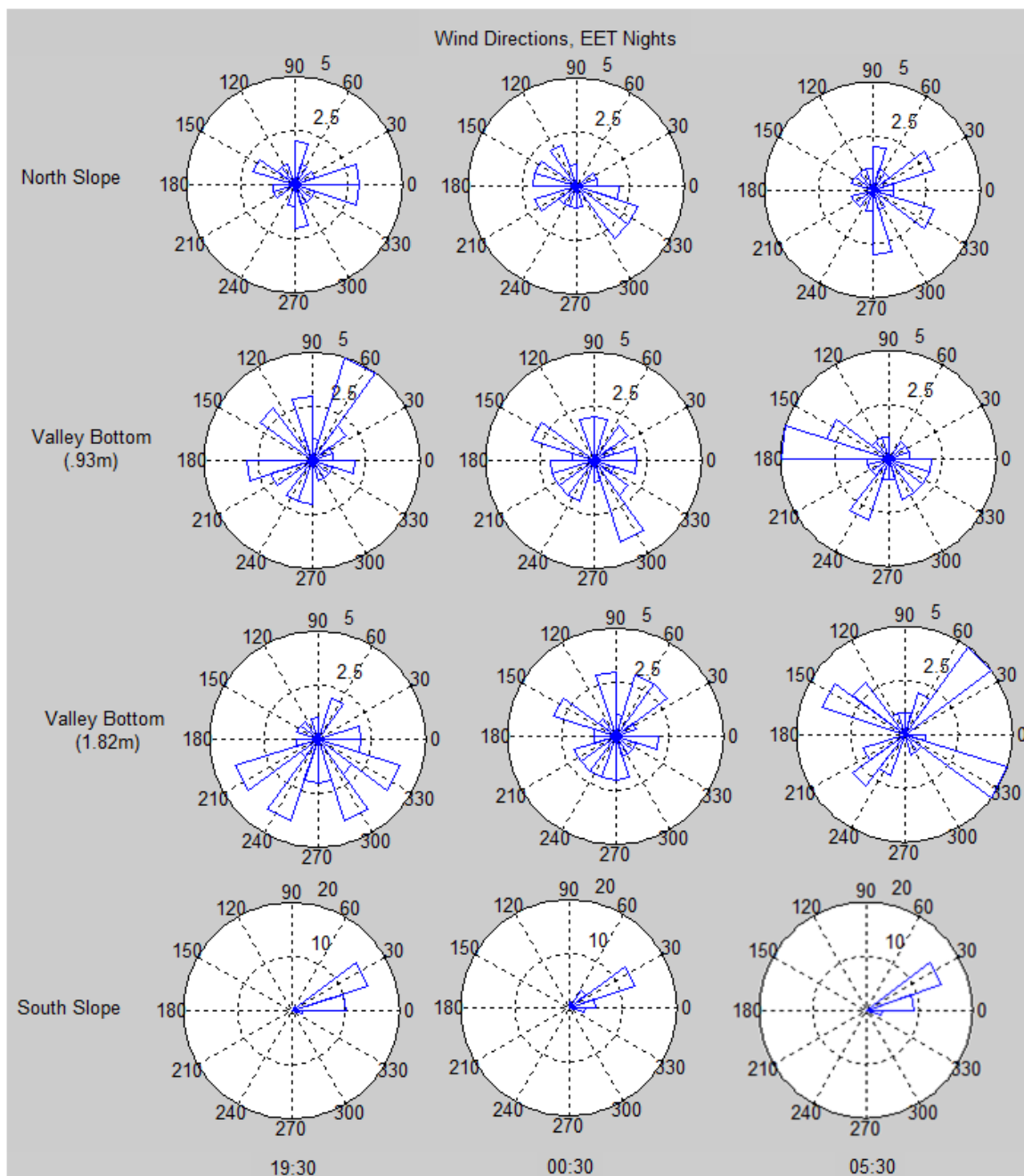
Figure 3-6. Composite wind roses at each of the sonic anemometer stations for representative times throughout EET nights. The bars point to the direction from which the wind is coming, and the length corresponds to the number of EET nights with that direction for that time. The valley outlet is to the West, which would be 180 on these plots.

Wind roses of the flow at each anemometer are shown in Figure 3-6. Composite wind

roses were calculated for each sonic anemometer site for each half hour throughout EET nights

and non-EET nights; what is shown here are the composite wind roses at three representative

times (during the EET, in the middle of the night, and before sunrise in the morning) for EET nights. These wind roses are analogous to circular histograms, and focus purely on direction rather than speed. The south slope anemometer shows persistent flow from the northeast on both transition nights and non-transition nights, whereas the other anemometers seem to show no persistent direction at any one point throughout the night. The downvalley flow is much more evident when we divide the wind directions into their components, as was done in Figures 3-3, 3-4, and 3-5. Non-EET nights look quite similar to EET nights, and since no significant insights are gained from them, that figure is not presented.

A few opportunities for error to be introduced in the wind measurements should be mentioned for completeness. The sonic anemometer was placed at .914m above the surface, which may have been too high to capture any shallow "skin flow" that would have formed by this point on the slope (Manins 1992). However, there are two anemometers at different levels on the valley floor that gave very consistent measurements throughout the study period. Also, the number of nights in the wind data samples is smaller than the number of nights in the temperature data sample. Several of the nights missing data showed a strong temperature pattern, so it is possible that the wind data collected is not representative of the transition nights as a whole. Finally, there is a small possibility that individual sensors could be affected by trees, infrastructure, or other blockages upstream in the flow. Though every measure was taken to situate the instruments in areas where the flow would not be blocked by existing vegetation, blockage cannot be ruled out as these instruments were located below the canopy in a forest.

In any case, it appears that the formation of a temperature pattern is not *strongly* correlated with the existence of downslope flow at the two slope sonic anemometers, since downslope flow is not evident in either transition or non-transition nights at either of the slope sonic anemometers, for any point throughout the night. Downvalley flow, which was an important variable to spatial temperature pattern formation by the BestFirst+CfsSubsetEval

algorithms, is evident on the south slope, but not as strongly on the north slope during transition nights and is clearly evident at both valley sonic anemometers.

3.2.3 Temperature Pattern Structure

Taking the difference between the average composite temperatures of each cluster every ten minutes yields dissimilarity in how these two types of nights evolve. The absolute value of the composite temperature difference between the two types of nights at ten-minute intervals is shown in Figure 3-7. During the first half of the night, during and slightly after when the EET is occurring (roughly until 0:00LST) the difference between the composited average is increasing, suggesting that the clusters are developing in a different manner. After 0:00, the difference between the composite average temperatures remains fairly constant, implying that the temperature patterns are evolving in a similar manner from this point onward. The spacing
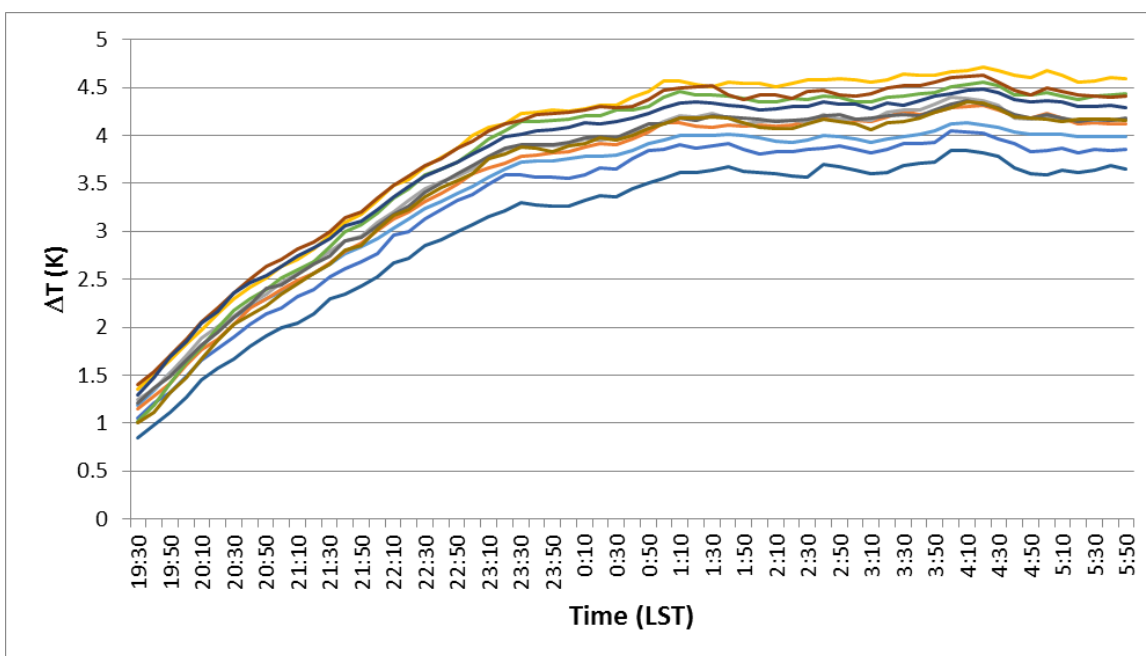
Figure 3-7. The absolute value of the composite temperatures on EET nights minus the composite temperatures on non-EET nights. The evolution of the cluster temperature difference shows that EET nights and non-EET nights evolve differently in terms of the temperature field.

between the contours for each temperature sensor suggests that a spatial pattern has been established in either one or both nights, for there is little change in the order of the sensors. The sensor represented by the line that is closest to the x-axis, for example, tends to always have the smallest difference between the two types of nights, which suggests that it always seems to have roughly the same temperature between EET nights and non-EET nights. This contrasts with the yellow line representing a sensor low on the south slope, which tends to have the largest difference between EET and non-EET nights only after the evolution of the difference between the two types of night stops. At the beginning of the night, the low south slope sensor is nearly indistinguishable from the other temperature measurements. This difference in ranking from the beginning to the end of the night suggests that the south slope sensor changes temperature relative to the other sensors in the network in addition to temperature changes overall. This figure shows that there is a difference in the spatial temperature distribution between transition nights and non-transition nights, and that EET nights show much more cooling of surface layer temperature early in the night.

The nature of the difference between the spatial temperature patterns in the two clusters was determined by a ranking analysis of the temperature sensors within the valley and converting the values into potential temperature to account for elevation differences between the stations. Figure 3-8: A-B show the average rank evolution of each potential temperature sensor on EET and non-EET nights. During transition nights, there is considerable change in the average rankings during the first half of the night followed by steadier average rankings during the second half of the night. This evolution suggests that much of the spatial temperature pattern setup occurs during and immediately after the early evening transition layer on transition nights. During the non-transition nights, there is much less of a change in the rankings during the first half of the night. Gradual changes do occur, but these changes do not seem to have a preferred time of night.
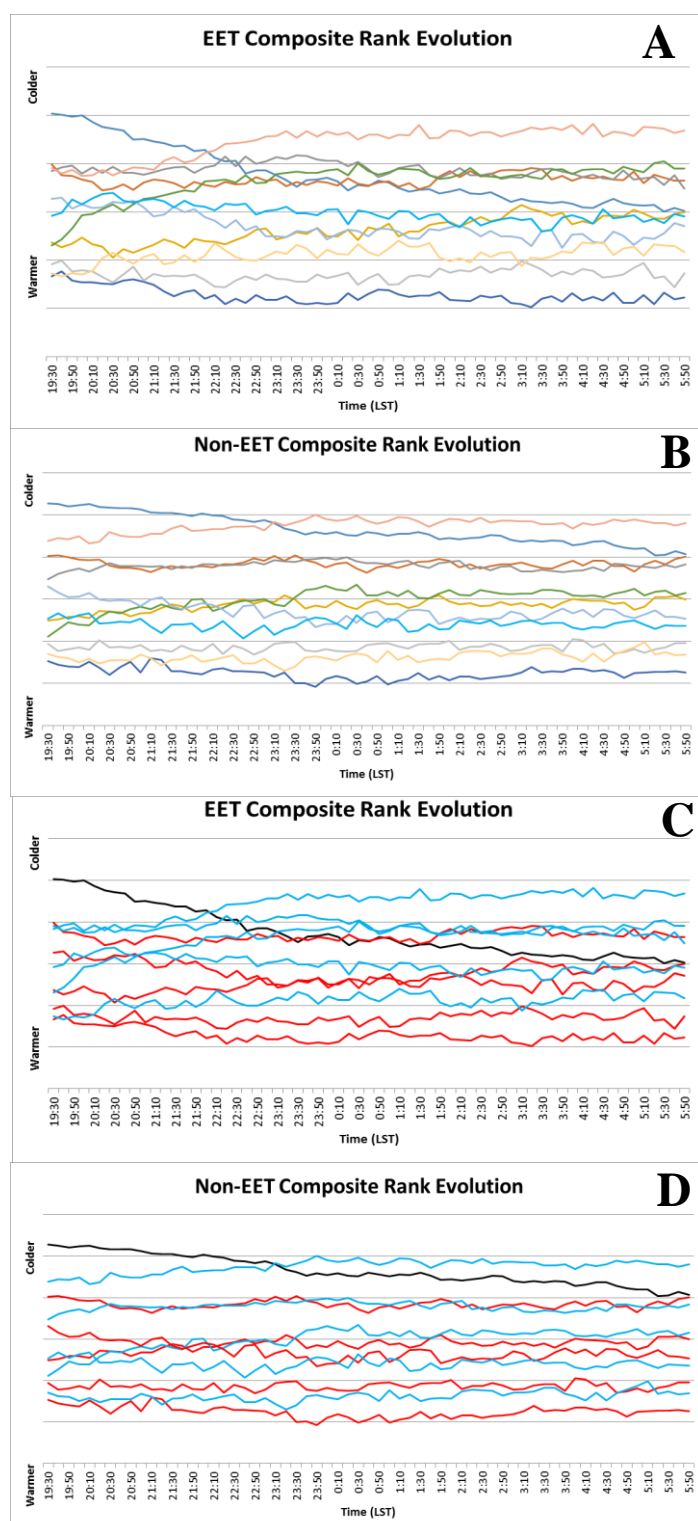
Figure 3-8. Rank of the sensors with respect to each other. A.) Potential temperature rank evolution on transition nights. B.) Potential temperature rank evolution on non-transition nights. C.) As in A, but color coded by slope. Blue lines indicate north slope sensors, red lines indicate south slope sensors, and the black line is the valley bottom sensor. D.) As in B, but color coded by slope

Figure 3-8: C-D are color-coded by location. The south slope sites are red, the north slope sites are blue, and the sensor at the valley bottom is black. With the topographic division, it becomes clearer that on transition nights the north slope sites tend to be colder than the south slope sites, while on non-transition nights the slopes are nearly indistinguishable by their rankings. The valley bottom also becomes much warmer, relatively speaking, on transition nights when compared to the other sensors in the micronetwork, as the black trace in Figure 3-8D moves closer to the x-axis and therefore warmer ranking as the night goes on.

Ranking frequency histograms for each sensor are displayed in Figure 3-9. EET

nights are indicated by blue bars, and non-EET nights are indicated by the red bars. In most cases, non-transition nights tend to have sharper peaks in their histograms, indicating higher repeatability of potential temperature rank occurrence at any given location. However, the distributions typically have similarly shaped distributions between transition nights and non-transition nights. The valley bottom temperature sensor, NPro1, has an unusual histogram in that it is bimodal between the extreme rankings on EET nights; it is usually either the coldest or the warmest sensor in the network. On non-EET nights, it tends to consistently be one of the coldest sensors. NPro2 and NPro3, located at the top of the south and north slope respectively, often have some of the coldest average temperatures in the network for both EET and non-EET nights. SA9, located at .914m at the top of the north slope, is usually the coldest location on non-transition nights, consistent with its location at the highest elevation of the network. There appears to be no difference on non-transition nights in ranking between the south slope and the north slope, nor between the sensors located at .914 m and the sensors located at .457 m. On transition nights, as is seen in Figure 3-8, the north slope is generally colder than the south slope, though there is no difference in ranking between the sensors located at .914m and the sensors located at .457 m.

From these histograms, we can see that there is a persistent spatial temperature pattern within the Shale Hills Critical Zone Observatory on both EET nights and non-EET nights. Sensors that are cold on one transition night are cold on other transition nights as well, and the same holds true with non-transition nights. Thus, we can conclude that the largest difference between transition nights and non-transition nights is the temperature pattern *evolution* and *structure*, rather than the outright existence or lack of a consistent temperature pattern. Non-EET nights may be more similar to one another than transition nights, which would point to topographic sheltering (both radiative and wind) as an important mechanism by which a spatial temperature gradient becomes established. Since the geographical features of the valley do not
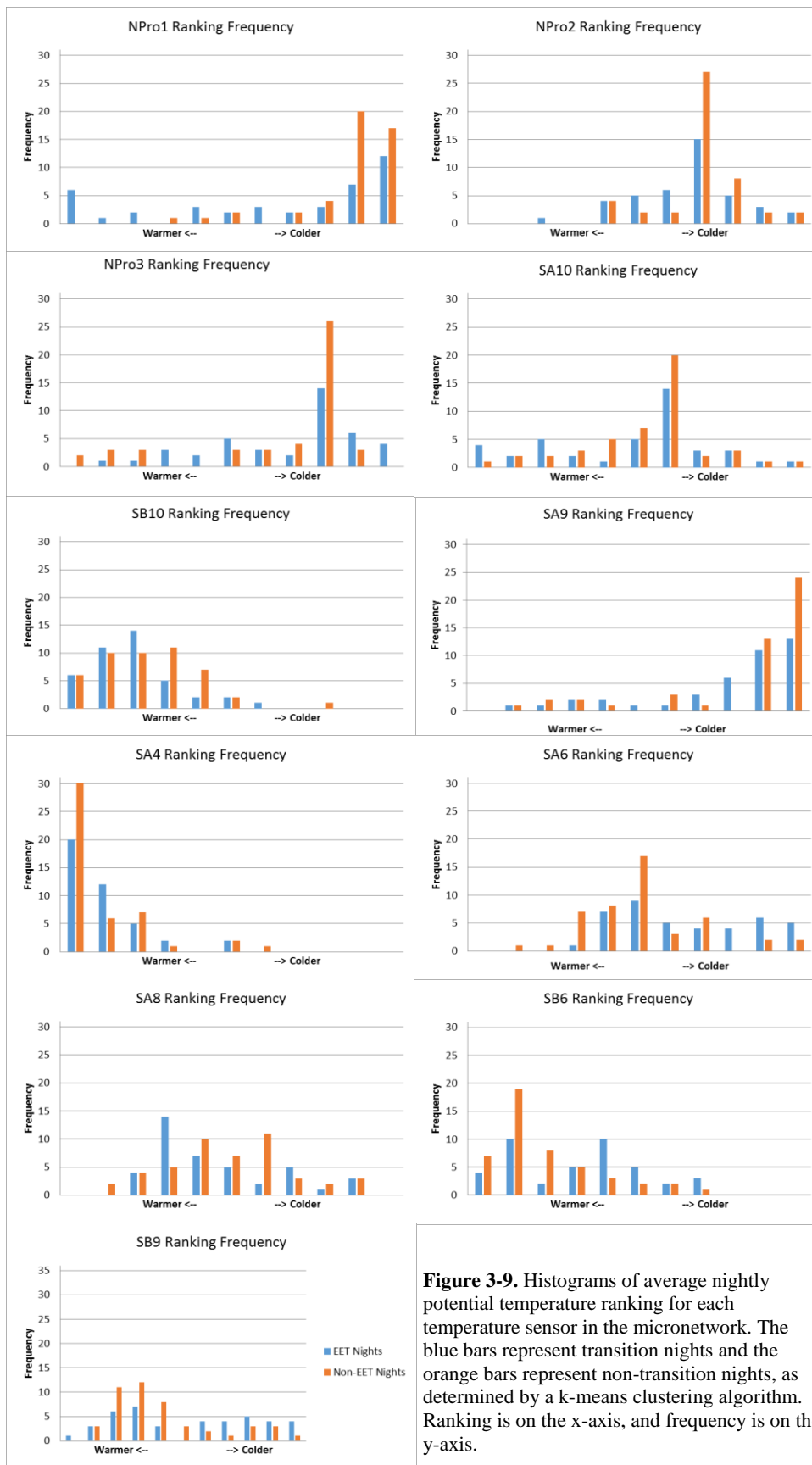
Figure 3-9. Histograms of average nightly potential temperature ranking for each temperature sensor in the micronetwork. The blue bars represent transition nights and the orange bars represent non-transition nights, as determined by a k-means clustering algorithm. Ranking is on the x-axis, and frequency is on the y-axis.

move, this sheltering effect would remain consistent and lead to higher peaks on the frequency histogram if it were the dominating influence on the temperatures for non-EET nights.

On EET nights, there is evidence for a down-valley drainage flow, which may work to redistribute the temperature pattern within the valley throughout the night and therefore redistribute the rankings of the individual sensors in the network. This redistribution would be difficult to capture through ranking histograms when they are ranked based on an average temperature throughout the night, since earlier it was suggested by the composite rank evolution plots that the change in the sensor rankings occurs across the EET period. The evolution that occurs on transition nights leads to a broader distribution of rank for any individual temperature sensor, since the average temperature across a night does not capture the nightly evolution of the temperature at any given point.

3.3 Large-Scale Environmental Conditions Associated with EET Observation

Large-scale environmental conditions play a significant role in determining whether a
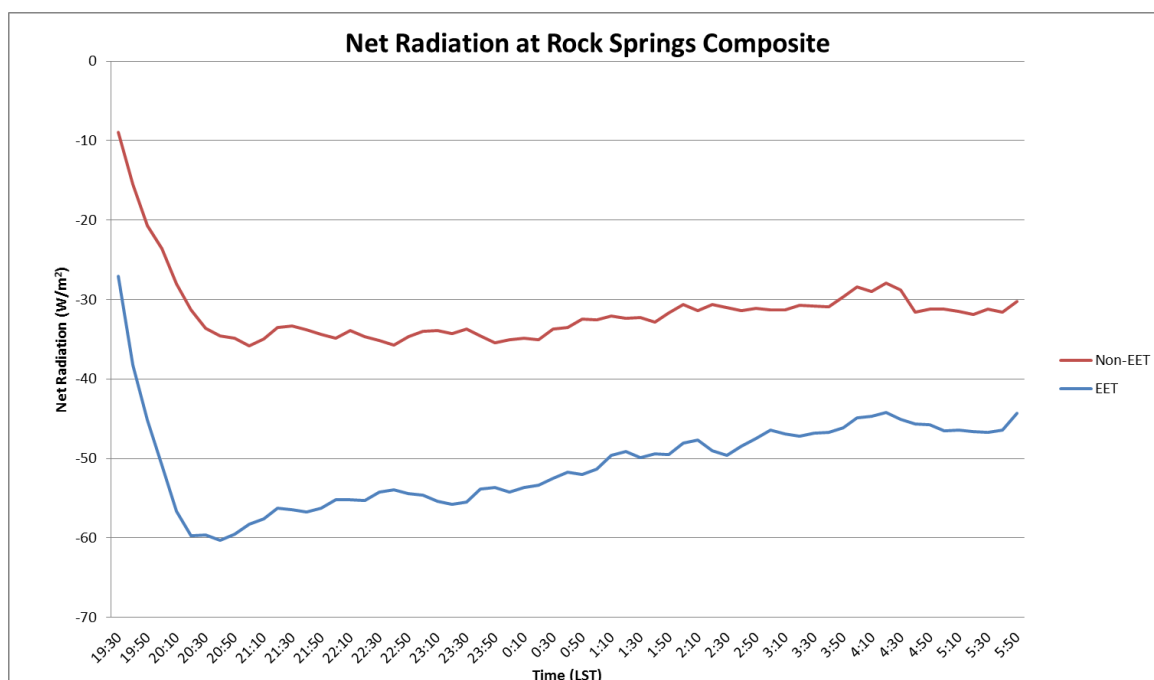
Figure 3-10. A comparison of the above-canopy net radiation evolution between pattern and non-pattern nights. Radiation data is taken from Rock Springs, an agricultural research site near Shale Hills operated by NOAA.

night is a transition night or a non-transition night. The k-means clustering algorithm identified both net radiation and above-canopy wind speed, prominent environmental variables, as important. As previously stated, calm, clear nights are conducive to drainage flows (Vergeiner and Dreiseitl 1987; Mahrt 1982; Fleagle 1950). Calm, clear nights also appear to be conducive to the onset of an EET period as observed at the Shale Hills Critical Zone Observatory. Net radiation showed a large difference between EET nights and non-EET nights, almost 20 W/m^2 in the averaged value of the net radiation across the night. The evolution of the net radiation in these two types of nights also differs, and is illustrated in Figure 3-10. Both transition nights and non-transition nights show a rapid decrease in net radiation, though transition nights show both a steeper decrease and a slightly shorter time of decrease. The differing average starting values likely relates to the difference in average start date between the two clusters. Transition nights occurred earlier in the calendar year on average than non-transition nights and so in a majority of those nights the net radiation had already been dropping for up to an hour prior to the analysis start time. However, these analysis times were chosen to exclude any measurements taken before sunset and consequently before the EET begun. Despite the initial difference at the start of the evenings, a difference of at least 10W/m^2 persists between the clusters throughout the night, even after the rapid decrease that occurs early in the night begins to level.

The large negative values of environmental net radiation reached on transition nights suggest that the sky is clear and that there is relatively less downwelling atmospheric infrared radiation heating the Earth. These measurements were taken at Rock Springs, an agricultural site near Shale Hills, so the increasing Leaf Area Index throughout the study period at Shale Hills would not have an impact on the above-canopy radiation measurements. Missing tower data at Shale Hills prevented the use of tower net radiation data for our analyses, but when data was present at both Shale Hills and Rock Springs, the comparison between them suggested that the

values were sufficiently close to be used for the purpose of this study. Differences were generally

15W/m^2 or less during the night.

Above-canopy wind speed was also composited by thirty-minute averages for transition

nights and non-transition nights to examine differences between them. These above-canopy wind

speeds were generally higher than those measured in the forest. Figure 3-11 shows the average

tower wind speed throughout the night on EET nights and non-EET nights. The non-transition

nights maintain a wind speed of ~2-2.5 m/s throughout the night, with no obvious trend or

evolution. However, the transition nights show a steady decline in average wind speed throughout

the night. The calming is steeper before midnight, during the EET, and becomes steadier

afterward. The second half of transition nights is much calmer than non-transition nights. These

calmer wind speeds could lead to decoupling of the flow near the surface, and may be correlated

with the downvalley wind observed at the subcanopy sonic anemometers.
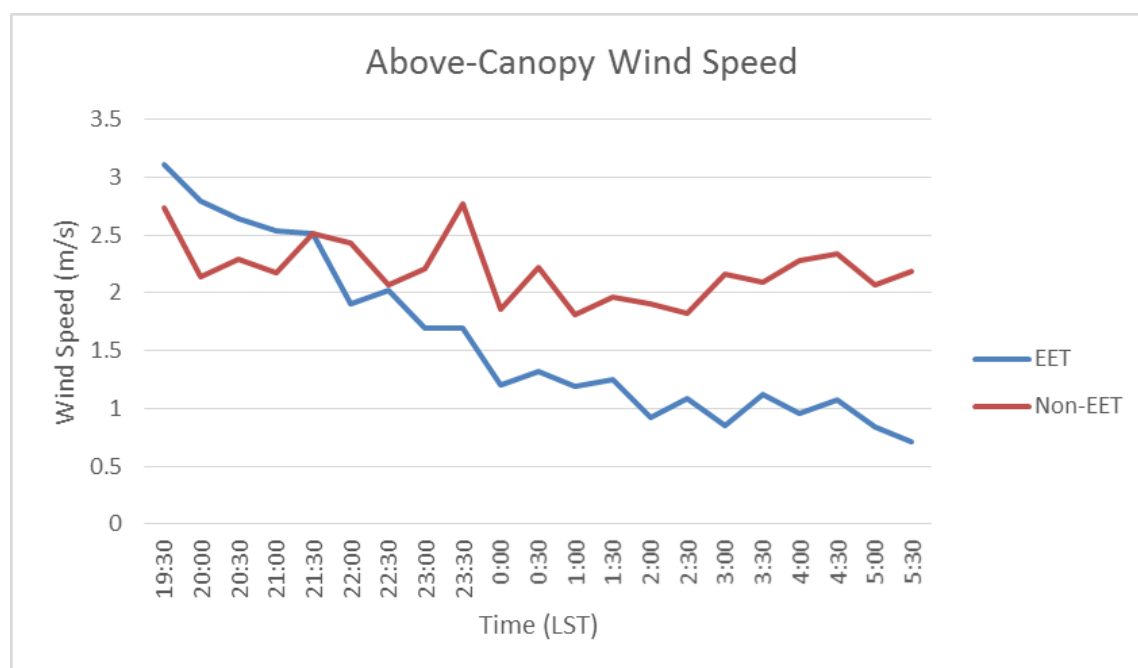
Figure 3-11. Composite 30m tower magnitude of wind speed for transition nights (blue) and non-transition nights (red).

The variability of above-canopy wind speed during transition nights and non-transition nights is illustrated in Figure 3-12. This figure shows the standard deviation of the measurements at each time within the particular groupings of EET nights and non-EET nights. At the start of the night, transition nights are not very similar to one another. However, as the night continues, transition nights become more and more similar to one another with regard to above-canopy wind speed. By the end of the nighttime measurement period, the standard deviation between the nights in the clusters is less than one meter per second. This growing similarity contrasts with the non-transition nights, which maintain a high intra-cluster standard deviation of the above-canopy wind speed. The standard deviation between the non-transition nights remains around three meters per second throughout the entire night and does not appear to follow any particular evolution. The similarity between transition nights indicates that the lowering above-canopy wind speed is indeed correlated with the formation of a spatial temperature pattern and existence of an EET affecting the below-canopy atmosphere. Low above-canopy wind speed has been shown to allow
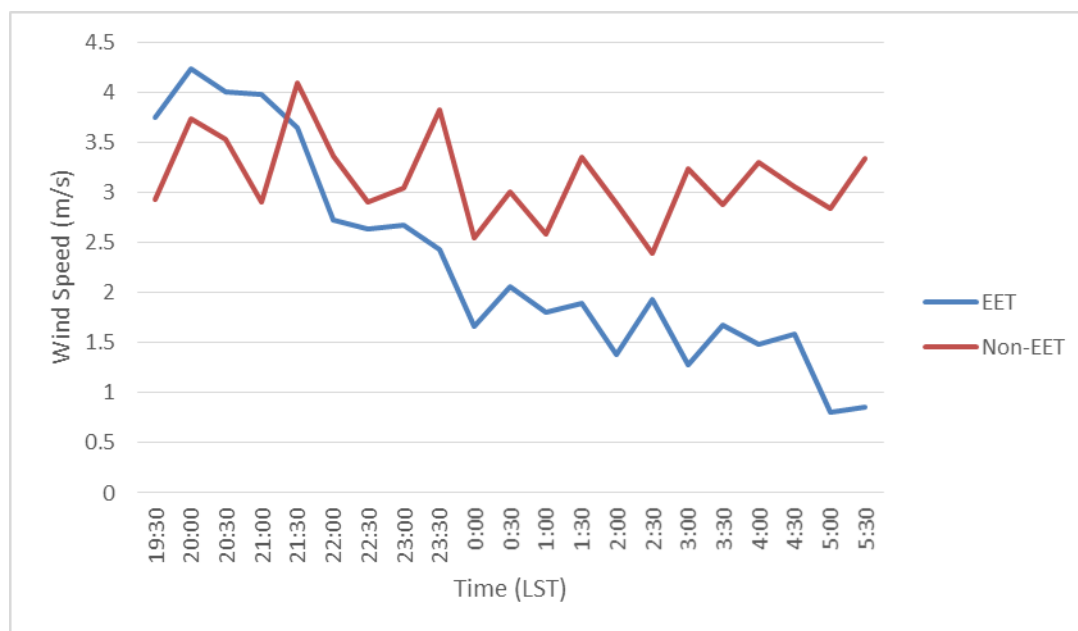
Figure 3-12. The time evolution of the intra-cluster standard deviation of wind speed for transition nights (blue) and non-transition nights (red). The standard deviation is of the half hour wind speeds of each night within the group of all EET or all non-EET nights.

for easier decoupling of the subcanopy flow (Turnipseed et. al. 2003) and in our case may assist in the establishment of the downvalley flow that was observed throughout the second half of transition nights.

3.4 Sub-Canopy Energy Balance Differences between EET and non-EET Nights

Typically, the change in potential temperature is estimated solely by

$$\frac{\partial \bar{\theta}}{\partial t} \cong \frac{R_{net}}{\Delta z}. \quad (4)$$

However, when the net radiation over a variety of depths is plotted against the change in observed potential temperature over time for an example case study (Figure 3-13), it becomes clear that this term alone does not account for the entirety of the observed change in potential temperature. If a constant Δz is assumed over time, smaller heights more closely estimate the observed rate of
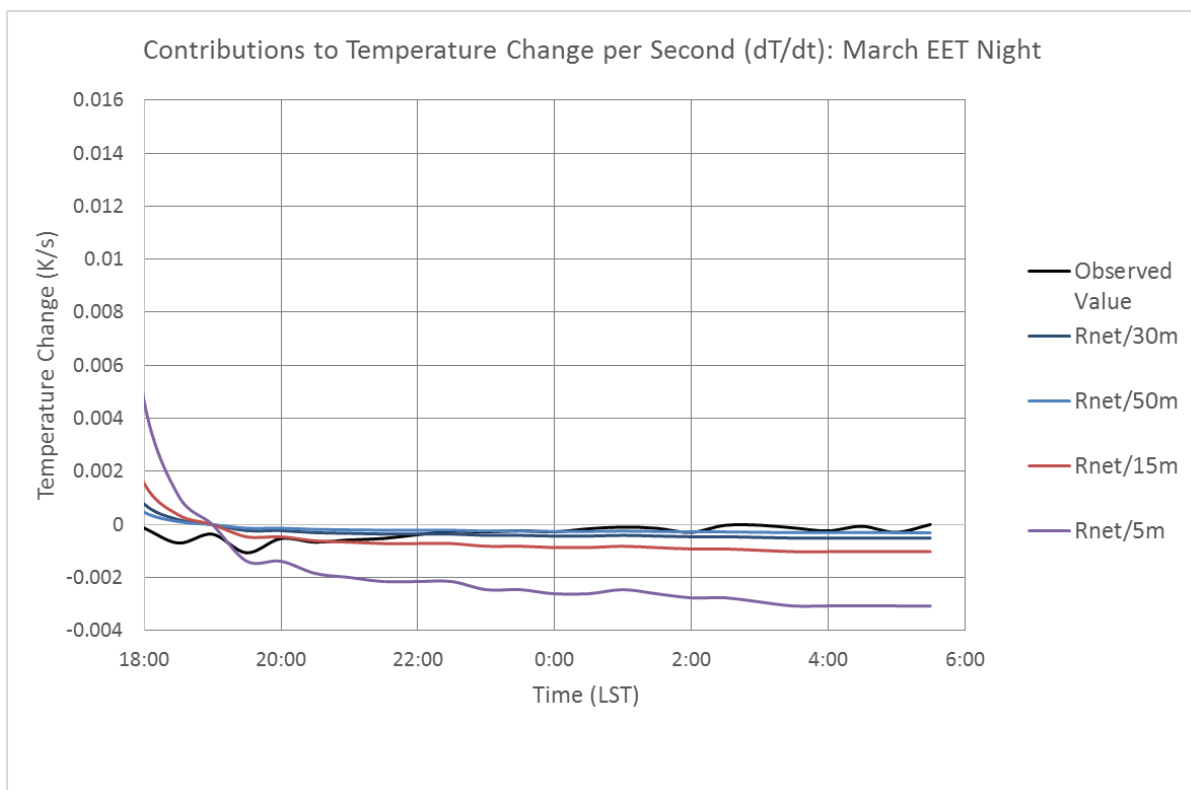
Figure 3-13. Predicted values of the temperature change in time based solely on net radiation divided by certain heights, compared to the observed value, which is denoted in black.

potential temperature change at the beginning of the night, and larger heights approximate the observed rate of cooling better during the second half of the night. However, no individual constant height explains the entirety of the observed rate of cooling, as is expected by the approximation made in Equation 4.

Additionally, if a collapse in turbulence just before the start of the EET causes the height over which the radiation is being distributed to sink, greater rates of cooling would be expected as the night goes on, due to a smaller area over which the net radiation is being distributed by the vertical and horizontal turbulent heat fluxes. However, the opposite pattern is visible in the observed cooling rates. Cooling is greatest at the beginning of the EET, and gradually decreases throughout the evening. However, direct measurements of the vertical and horizontal turbulent flux divergences were obtained in this study, and so these directly measured turbulent flux divergences can be compared to the observed rate of cooling. This comparison will allow determination of which terms are thwarting the validity of the assumptions made by Equation 4, and provide greater insight into the mechanisms of cooling at Shale Hills.

The measurement of three-dimensional winds, radiation, and temperature at multiple sites of varying spatial location and elevation allow for the direct calculation of many terms in the energy budget from measurements. The terms that we were able to directly calculate are highlighted in red in the simplified surface layer energy balance equation,

$$\frac{\partial \bar{\theta}}{\partial t} + \bar{u}\frac{\partial \bar{\theta}}{\partial x} + \bar{v}\frac{\partial \bar{\theta}}{\partial y} + \bar{w}\frac{\partial \bar{\theta}}{\partial z} = -\frac{\partial \overline{(u'\theta')}}{\partial x} - \frac{\partial \overline{(v'\theta')}}{\partial y} - \frac{\partial \overline{(w'\theta')}}{\partial z}, \quad (5)$$

where θ is the potential temperature, u, v, and w are the three components of the wind, $u'\theta'$ is the valleywise heat flux divergence, $v'\theta'$ is the slopewise heat flux divergence, and $w'\theta'$ is the vertical heat flux divergence. Bars indicate averaged terms and primes indicate perturbation terms. Highlighted in blue is the term we are trying to explain – the cooling rate at the valley bottom. Independent measurement of the cooling rate at the valley bottom allows evaluation of

the budget and determination if the calculated budget reflects the actual cooling rate measured at the valley floor.

Examination of these terms will also provide further characterization of EET nights and which terms are influencing the decrease in temperature. The two sonic anemometers at the valley bottom allow for estimates of the vertical advection and vertical heat flux divergence. Horizontal advection in the slopewise direction and horizontal heat flux divergence in the slopewise direction are able to be calculated using three combinations of slopes: the north slope and valley bottom, the south slope and valley bottom, and the north slope and the south slope.

Net radiation measurements taken directly at the slope sites show the influence of the canopy increasing throughout the study period. The temperature and wind measurements at the tower suggest that the tower was decoupled from the valley flow on both EET and non-EET nights via stability (see Table 4 and Figure 3.11).

The first sub-section of this section discusses composite fluxes measured for all EET and non-EET nights. For complete calculation of the budget, the terms were small enough that one outlier on either EET nights or non-EET nights could easily influence the entire budget for that cluster if the surface layer energy budget were computed for composites, as this study has done until this point. Thus, for calculation of the budget, case studies of one EET night and one non-EET night occurring one or two nights apart from one another were used to calculate a full budget and determine which nights were important to the final predicted change in temperature. Description of the relevant case studies will comprise the second sub-section of this section, and an analysis of the energy budget will conclude the section.

3.4.1 Composited Fluxes

When determining terms of the sub-canopy energy balance, fluxes needed to be
calculated at each sonic anemometer in order to compute the flux divergences for each direction.
These fluxes were then composited and examined for differences between the terms. Vertical heat
fluxes, illustrated in Figure 3.14, showed the largest differences between EET nights and non-
EET nights, particularly at the two valley bottom sites and at the north slope site. At these sites,
the EET nights showed stronger, more positive heat flux than non-EET nights during the first half
of the night – from the EET period until approximately midnight. This corresponds with both the
upward motion of warm air and the downward motion of cold air. The intra-cluster standard
deviation of these measurements is approximately twice as large as the mean, but the trends that
emerge when the fluxes are composited agree with our intuition that we would see a difference in
the vertical heat flux at most of the locations during the first half of the night between EET and

Figure 3-14. Composite vertical heat fluxes for EET nights (blue) and non-EET nights (red) at each of the four sonic anemometer stations.

non-EET nights, since cooling was observed at the surface.
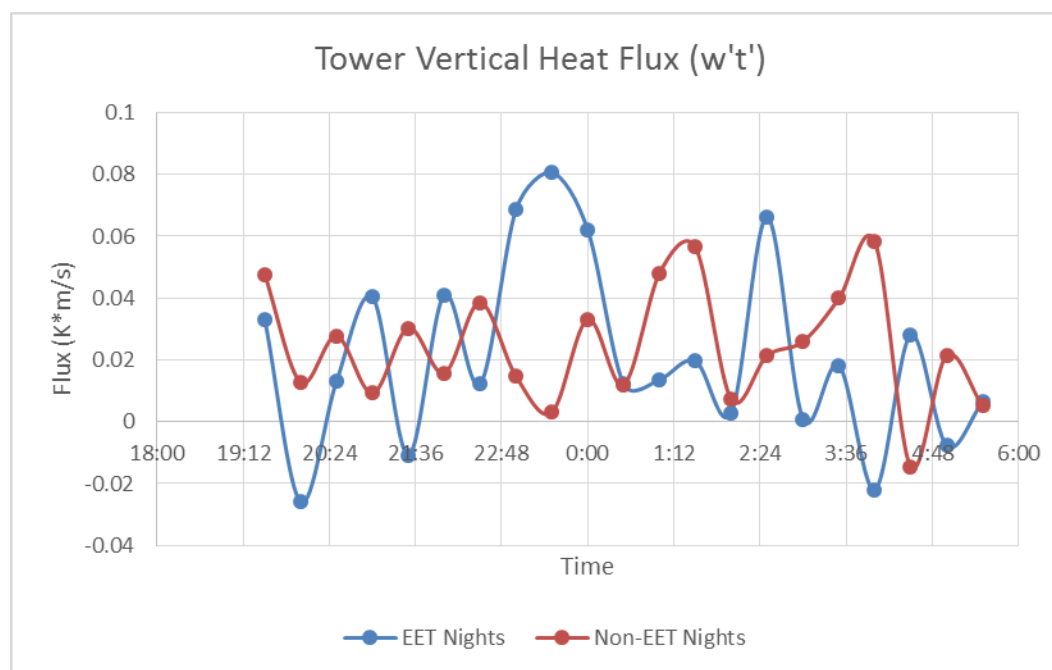
Figure 3-15. Composited vertical heat flux at the tower sonic anemometer for EET nights (blue) and non-EET nights (red).

When these heat fluxes are compared to the tower vertical heat flux (Figure 3-15), two things stand out. First, the magnitude of the tower fluxes are larger than those found in the valley. More importantly, there is no obvious difference in the composites of EET nights and non-EET nights in the tower data during the first half of the night. The smaller magnitude of flux corresponds well with the general decrease in wind speeds that is seen at the tower on EET nights (see Figure 3-11), but the noise level in Figure 3-15 is large enough that the differences are likely not significant.

3.4.2 Case Study Descriptions

Three different case studies were examined to determine which components of the energy budget were the largest contributors to the overall cooling rate that is being estimated. Two case

studies taken from the beginning of the study period (March) and the end of the study period

(June) compared EET nights with conventional non-EET nights: nights where almost no cooling

took place. These two pairs of nights allowed us to see how the surface layer energy balance

might change from the cold season to the warm season. The third pair of nights is taken from

May, and the EET night is compared to a less conventional non-EET night, where it appears from

the temperature trace that an EET was begun multiple times before being perturbed away from

the uniform network cooling seen throughout the EET. Appendix A shows temperature traces for

each pair of nights; the difference between the March/June pair of nights and the May pair of

nights becomes clearer when comparing the temperature traces on the non-EET nights for each

case.

Net radiation on the north slope for each pair of nights is shown in Figure 3.16 A-B. The

net radiation on the south slope for each pair is shown in Figure 3.16 C-E. North slope data for

the March case study were unavailable due to instrument malfunction. These figures illustrate

several differences: the difference between the slopes, the difference in below-canopy net

radiation between EET nights and non-EET nights, and the effect of the canopy on the trunk

space net radiation. The difference between the slopes can best be seen in their magnitude of

negative net radiation. Generally, the south slope experiences less negative net radiation then the

north slope. This is in agreement with the rank analysis result that paints the north slope as the

cooler of the two slopes. The difference between EET nights and non-EET nights is also fairly

obvious. EET nights have more negative net radiation than the non-EET nights for these

particular nights, in agreement with the composite plots of above-canopy radiation that show

more negative net radiation for EET nights than non-EET nights.

The May case study (A and D) shows three marked decreases in the negative net

radiation on the non-EET nights. These dips occur when the May non-EET night appears to begin

attempting an EET period, suggesting that initiation of an EET period may require a decrease in

net radiation. The below-canopy net radiation is then clearly a key component of the below-canopy energy budget which leads to the EET and the subsequent uniform cooling. Comparing the below-canopy radiation between the beginning of the study period and the end of the study period, as illustrated by the March and June case studies, shows very little obvious difference. On the non-EET nights in both of these cases, there is roughly zero net radiation. On the EET nights, there appears to be a small difference in the magnitude of the negative net radiation, but it is perhaps not so great as we would expect considering that the March case study took place when

Figure 3-16. Net radiation data for three selected case studies. A-B are north slope net radiation for the May and June case studies respectively. C, D, and E are the south slope net radiation for the March, May, and June case studies, respectively. The EET night of each pair is denoted in blue, and the non-EET night is denoted in red.
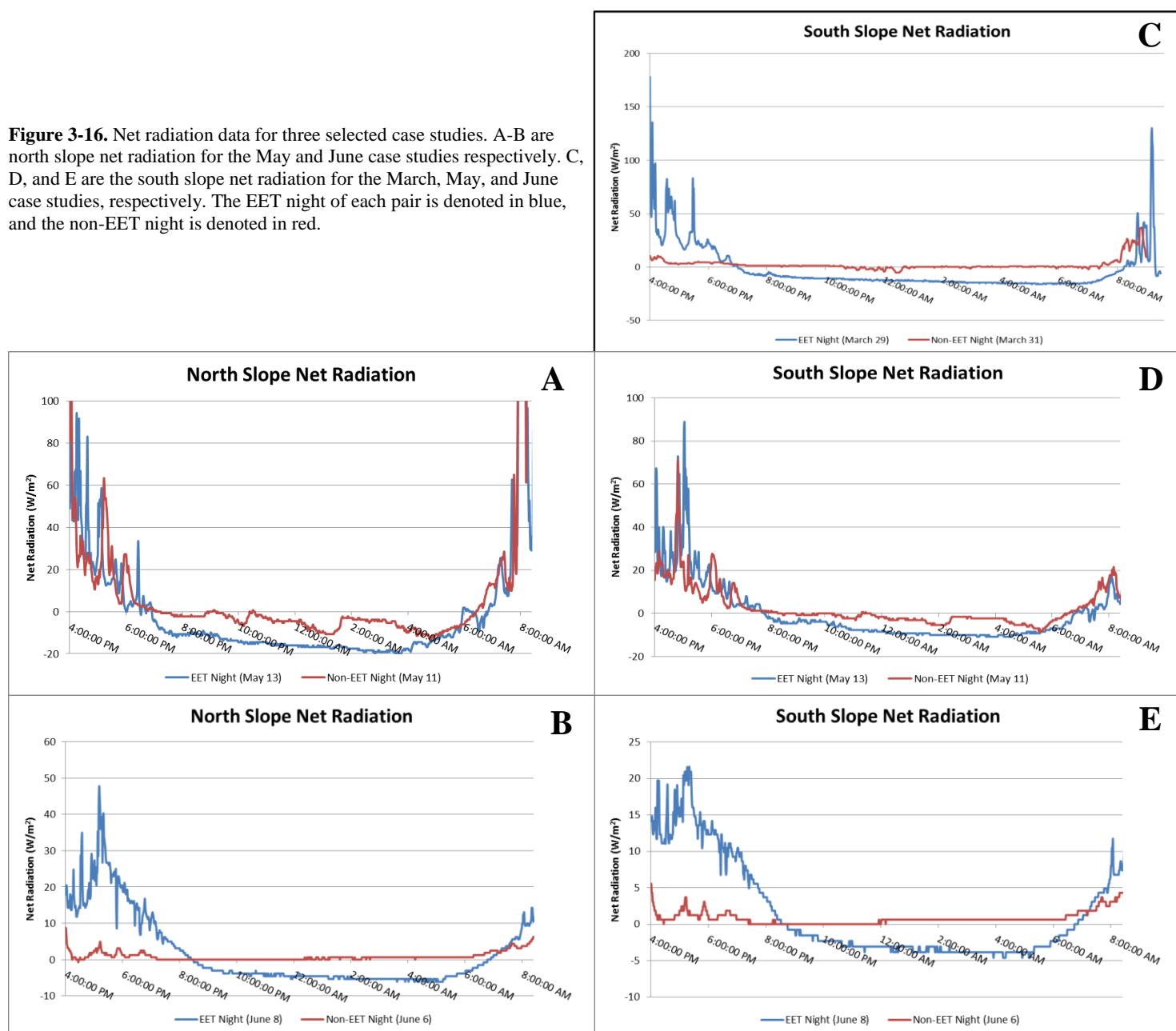
Shale Hills was in a time of leaf-off, while the June case study took place when Shale Hills was in a time of leaf-on.

Figure 3.17 shows the 30-min-averaged heat fluxes in the slopewise ($\hat{y}$), valleywise ($\hat{x}$), and vertical ($\hat{z}$) directions, as well as the momentum flux calculated using the valleywise and vertical winds (u'w') for the March case study – both the EET and non-EET night. The EET night is indicated by solid lines, and the non-EET night is indicated by dashed lines. Red lines are the valley bottom station at .914m, green lines are the valley bottom sonic anemometer at 1.83m, and the blue lines are the south slope sonic anemometer, which is located at .914m above the surface.
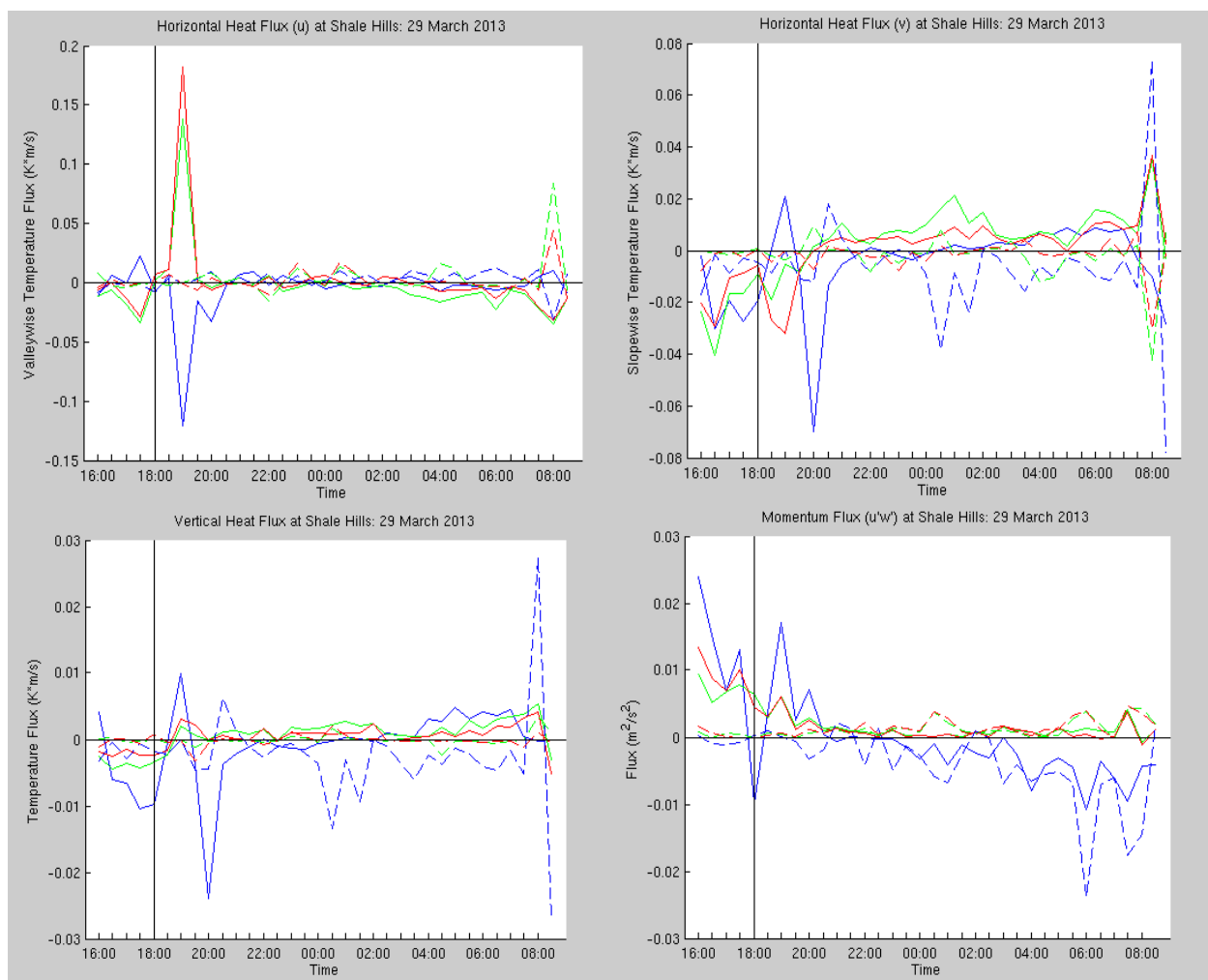
Figure 3-17. Calculated fluxes for the March case study. The EET night (March 29th) is indicated by solid lines, and the non-EET night (March 31st) is indicated by dotted lines. Red lines are the valley bottom station at .914m, green lines are the valley bottom sonic anemometer at 1.83m, and the blue lines are the south slope sonic anemometer, which is located at .914m above the surface. The vertical black line signifies the start of the EET, as determined by the network temperature traces.

As we expect, there is close agreement between the red and the green lines, which suggests that features on the valley bottom are being resolved. If these measurements had a large component of random noise, we would not expect such agreement between the two valley bottom anemometers. This correlation is a good check on our accuracy, since the fluxes being measured here are very small and we could suspect that instrument noise dominates our calculations. However, the independent sampling of what is likely the same eddy and agreement between two sonic anemometers suggests that instrument noise is not causing significant error in our fluxes.

A large spike can be seen in the horizontal heat flux in the valleywise direction at the beginning of the EET on the EET night, when the greatest magnitude of cooling is taking place. The spike is seen in both the valley bottom and the south slope anemometer, suggesting that this large flux is occurring across the entire network. Once the EET has passed, the fluxes remain quite small, although in general there are larger magnitudes of fluxes on the EET nights than on the non-EET nights. One exception to this is the vertical heat flux on the non-EET night, which remains relatively large throughout the night. Momentum fluxes decrease once the EET is through (at about midnight), and the average momentum flux on the south slope switches sign, suggesting that there is organized flow taking place. The non-EET night also shows increasing magnitude of momentum flux, but it has much larger variability than the EET night.

The June nights tell a similar tale with regards to flux. The north slope (south-facing slope) sonic anemometer was available in addition to the sonic anemometers shown in Figure 3.17, and is indicated by the black lines in Figure 3.18. Similarly to the March case study, there are generally larger-magnitude fluxes on EET nights than on non-EET nights, although the fluxes are for the most part small in all cases. The slope stations bear little resemblance to each other except in sign, and the sign differences between the slope and the valley bottom anemometers is due to differing alignments. Overall, the June nights show smaller-magnitude fluxes than the

March nights. Mostly, we have zero temperature fluxes everywhere, except for the vertical heat fluxes at the valley bottom on EET nights. These fluxes are small but positive, which is consistent with the earlier, composite results.

These two cases look very similar to one another, but they contrast greatly with the May case studies. In the May case studies, recall that the EET night and the non-EET night were much more similar, for it appeared that the non-EET night began a cooling period characteristic of the EET multiple times during the night, but was unable to finish it. The times of these cooling periods can be aligned with the flux plots to determine if corresponding increases in fluxes on the
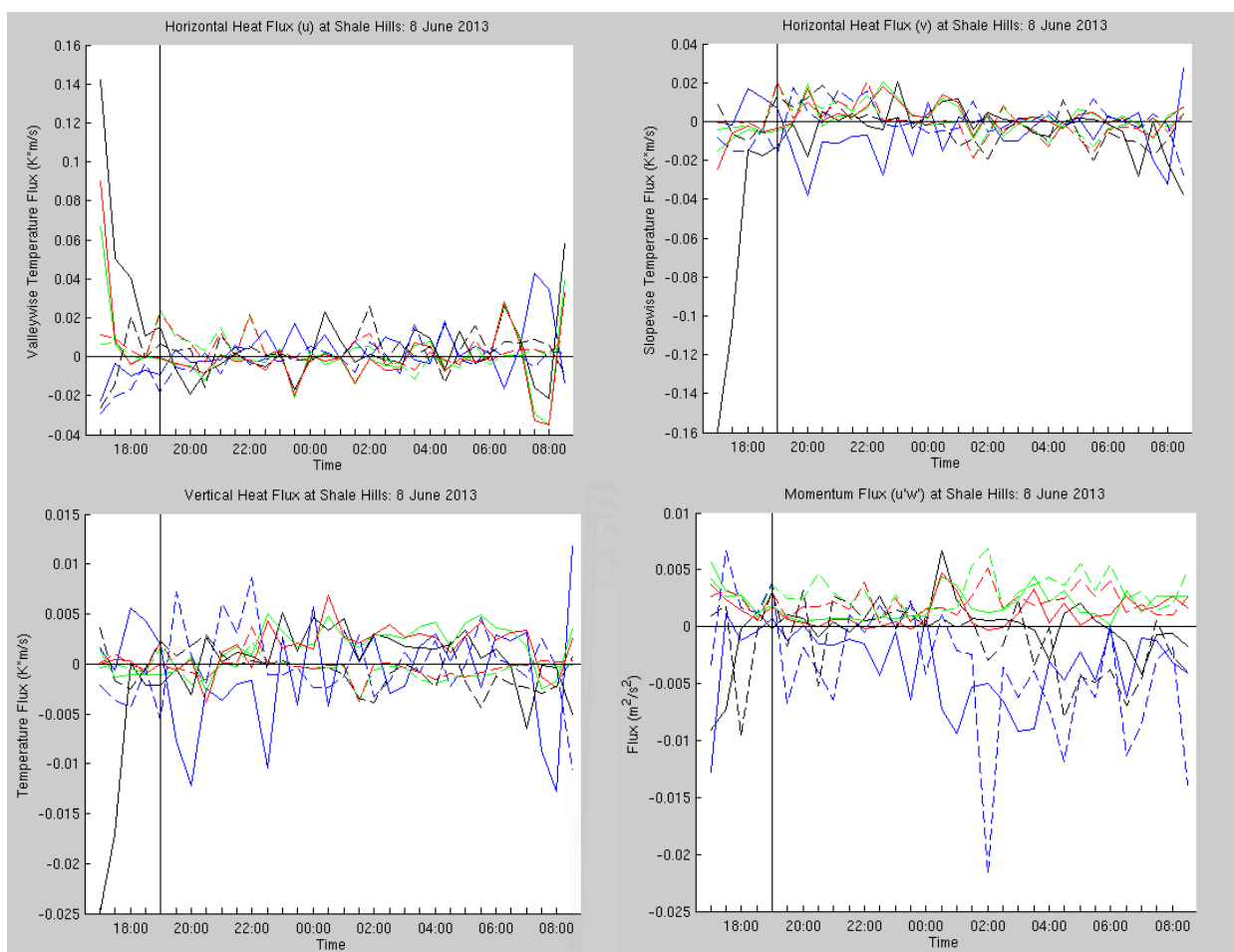
Figure 3-18. Calculated fluxes for the June case study. The EET night (June 8th) is indicated by solid lines, and the non-EET night (June 6th) is indicated by dotted lines. Red lines are the valley bottom station at .914m, green lines are the valley bottom sonic anemometer at 1.83m, black lines are the north slope sonic anemometer and the blue lines are the south slope sonic anemometer. Both slope anemometers are located at .914m above the surface. The vertical black line signifies the start of the EET, as determined by the network temperature traces.

non-EET nights occur around the time of the cooling. If so, we can conclude that the fluxes are important in distinguishing the EET portion of the night and contribute to explaining the spatial temperature pattern that sets up on EET nights.

Figure 3.19 shows the three heat fluxes and the momentum flux at each sonic anemometer for the May pair of dates. Similarly to the previous graphs, the solid lines correspond to the EET night (in this case, May 13th) and the dashed lines correspond with the non-EET nights (in this case, May 11th). The vertical black line, also as in the previous two cases, corresponds to the time of the EET's onset as determined by the temperature traces. However, the May case study nights have two vertical red lines. These lines have significance only with regards to the non-EET (dashed) lines; they correspond to two times during the non-EET night where the temperature traces appeared to signify the entrance into an EET period. These EET periods were not allowed to run to completion, for before they could result in differentiated temperatures, they were disturbed by turbulence or other forces, which can be seen on the temperature traces in Appendix A as a sudden plateauing or increase of temperatures immediately after an EET cooling.

Large spikes in the valleywise ($\hat{x}$) heat fluxes occur about an hour and a half after the onset of the EET night on May 13th, and we can also see a smaller-magnitude spike in the non-EET nights approximately 1-2 hours after the cooling periods. The slopewise ($\hat{y}$) fluxes are not extremely informative, although there also appears to be a spike in the non-EET night 1-2 hours after the onset of EET-like cooling. The momentum fluxes (u'w') approach zero, reflecting the calming of below-canopy winds throughout the evening. The convention of these two red lines will be kept on subsequent plots, to determine using the sub-canopy energy budgets whether these two cooling periods resembled the EET in any components of the energy budget. These fluxes suggest a decrease in the small positive flux later in the night, which could be part of why the cooling rate shifts.
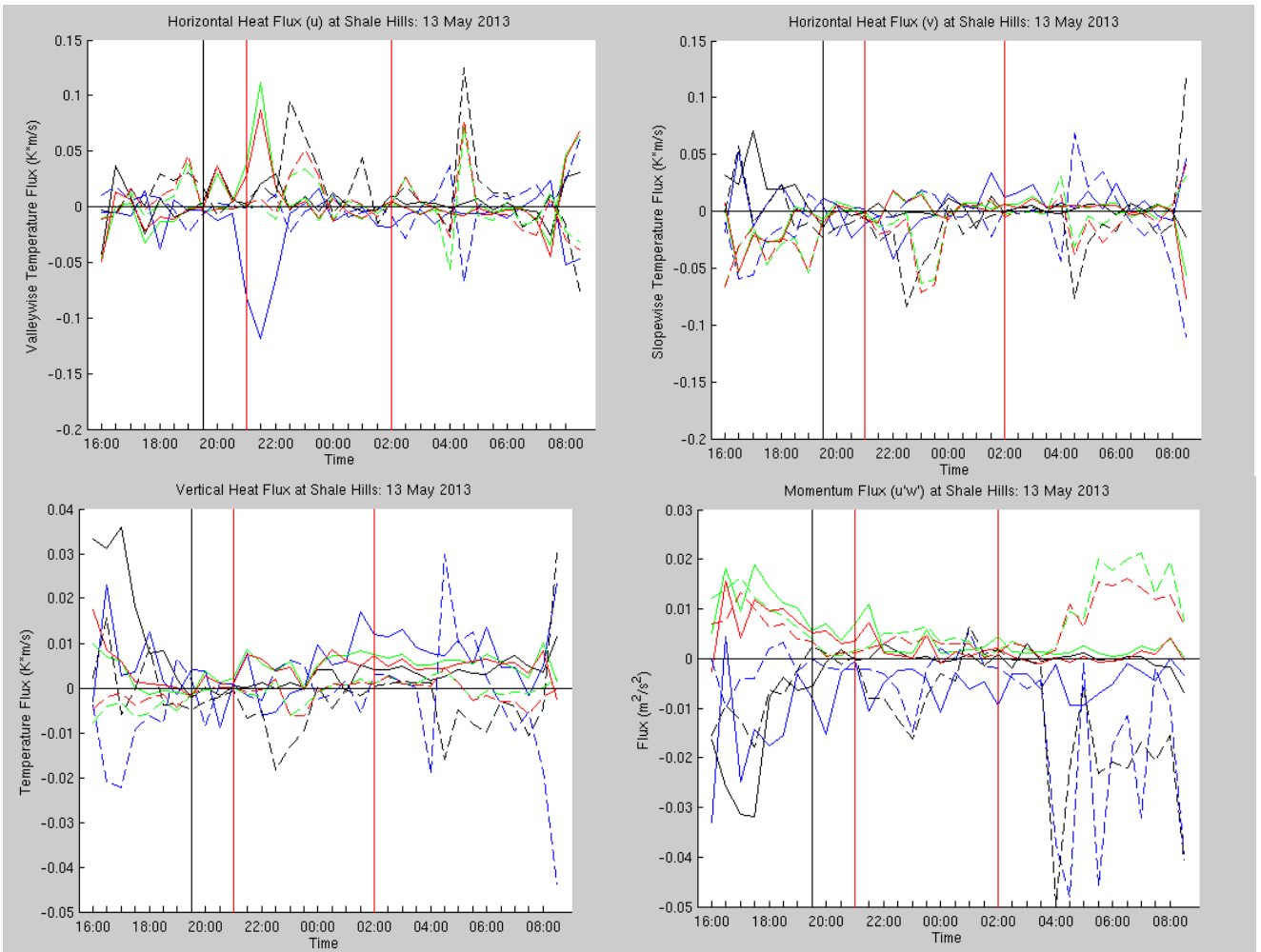
Figure 3-19. Calculated fluxes for the May case study. The EET night (May 13th) is indicated by solid lines, and the non-EET night (May 11th) is indicated by dotted lines. Red lines are the valley bottom station at .914m, green lines are the valley bottom sonic anemometer at 1.83m, black lines are the north slope sonic anemometer and the blue lines are the south slope sonic anemometer. Both slope anemometers are located at .914m above the surface. The vertical black line signifies the start of the EET, as determined by the network temperature traces and the red vertical lines signify times during the non-EET night when EET-like cooling began to occur.

3.4.3 Analysis of Sub-canopy Energy Budget

Table 5 lists the results of the energy budgets averaged over the entire night as compared

to the observed dT/dt at the valley bottom for each pair of EET and non-EET night studied.

Clearly, in this case the full budget does not do a good job at predicting the average rate of

cooling at the valley bottom. When the budget is broken into its component parts and examined

over the course of the night, it can be determined which of the terms is unstable and therefore

might not be as well-resolved as is ideal when calculating an energy budget. Figure 3-20 shows

the contributions to the temperature change per second by each of these terms when they are

examined every half hour across the night.

Average Budget Cooling Results		
Date	Full Budget dT/dt (K/hr)	Observed dT/dt (K/hr)
March EET	.252	-1.074
March Non-EET	150.306	0.146
May EET	1.135	-1.042
May Non-EET	9.355	-0.644
June EET	33.208	-0.830
June Non-EET	-139.729	-0.434

Table 5. Cooling predicted from the various components of the energy budget on each of the case study nights examined as compared to the actual measured average cooling rate at the valley bottom temperature sensor.

From these figures, it can be seen that in every case the vertical advection has a large

contribution to the value of the energy budget. The vertical advection is also a noisy term, and

fluctuates on both the EET and the non-EET nights. This fluctuation and large value may be due

to the distance over which the advection is being calculated – it is only .914m, so large

differences in temperature are amplified by dividing by the small distance. It can also be seen

from these plots that the vertical advection remains noisy throughout the night. Vertical advection

does not appear to change behavior between the EET portion of the night and the 2nd regime of

the night with a stable, uniformly cooling spatial temperature pattern across the valley. It is a

noisy term on both EET nights and non-EET nights and results in very unrealistic cooling rates.

Thus it is concluded that the vertical advection estimates derived in this manner are suspect, and

that examination of the budgets without the vertical advection term could prove useful in

differentiating which terms are important to causing the EET period.

Averaged budgets across the entire night may be sufficient for non-EET nights, but when examining the temperature traces of these case studies in Appendix A, it is easy to see that EET nights appear to have two different regimes. The period of rapid, uniform cooling that occurs directly after sunset is the EET period, and what we classified these nights according to. However, the cooling regime after the EET period, where a spatial temperature pattern is established across the network and the cooling rates are much slower is an entirely different regime and should be examined separately than the transition period.

Table 6 aims to address both the question of regime separation and the problems of the vertical advection. In Table 6, values of the full energy budget and the energy budget without the $\bar{w}\frac{d\bar{T}}{dt}$ term are contrasted with the measured dT/dt at the bottom of the valley for the transition time and the cooling regime that occurs after the transition period on ETT nights. These regimes were determined by the onset and end of the rapid cooling, and therefore encompass a different number of half-hour samples for each case study. Since there is only one regime on the non-EET nights according to our interest (there may in fact be multiple regimes, but the focus of this study is the EET and the driving forces behind it), the measured dT/dt will be the same as the values in Table 5. All the non-EET values in both Table 5 and Table 6 are the values for the full energy budget and are in K/s.

Removing the effects of the vertical advection term, which was often an order of magnitude larger than the other terms on EET nights, corrects the sign for most nights, with the exception of the June non-EET night. It also brings the predicted values to much more reasonable numbers, rather than the order 35K/half hour values that were previously seen with the inclusion of the vertical advection term. Indeed, for all of the EET nights, neglecting the vertical advection term brings the budget closer to the observed values. The neglecting of the vertical advection also brings the budget closer to the observed values in all of the EET nights during the quickly
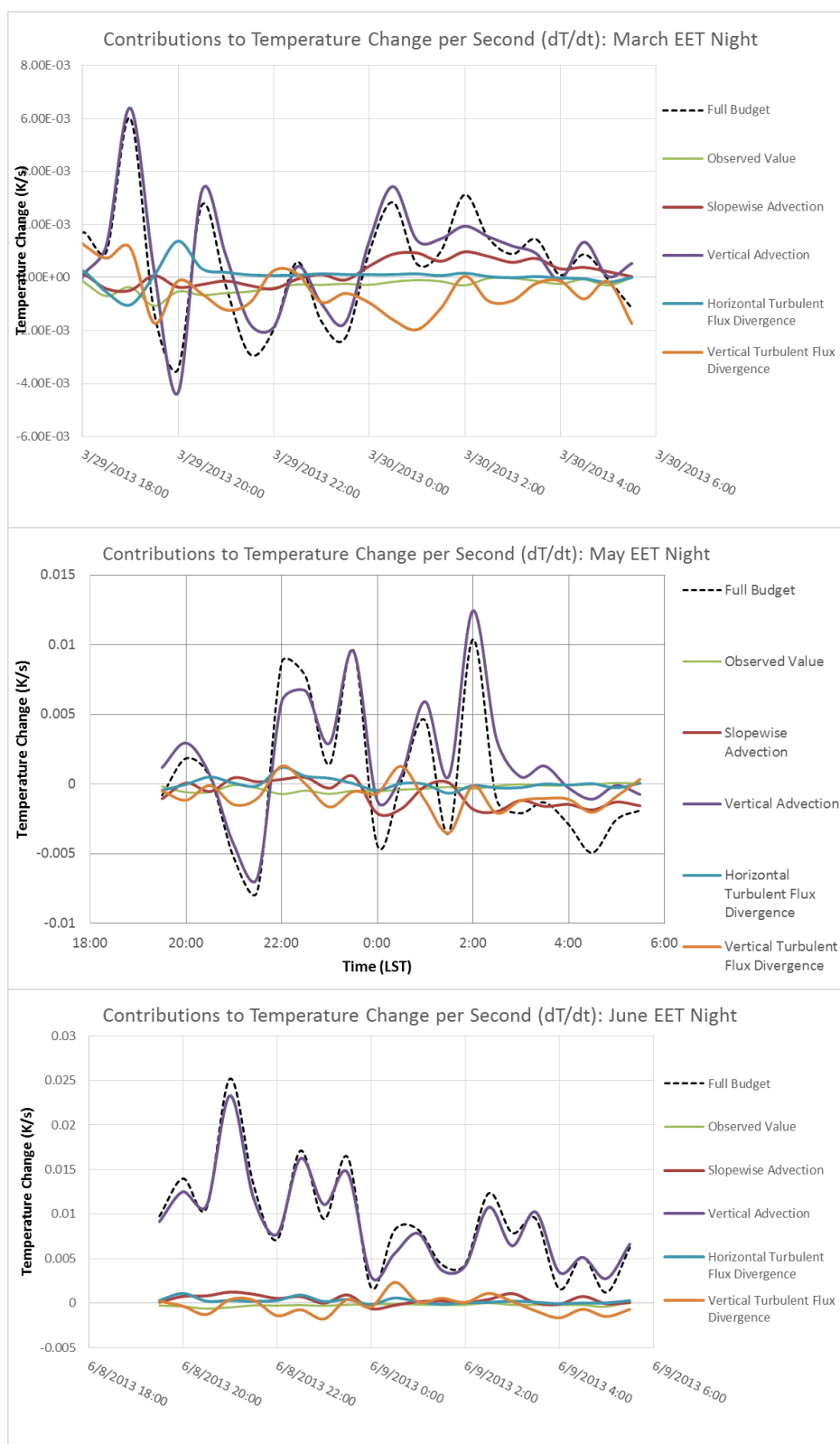
Figure 3-20. Contributions of each part of the surface layer energy budget to the total cooling rate for the EET nights in March, May, and June case studies. The full budget is denoted by a dashed line, while the contribution to the full budget from each term is denoted by a solid line. The observed cooling rate is in green.

cooling regime. It also brings the calculated values closer to the observed values in two of the

three second, more steady regimes. Overall, neglecting the vertical advection term solves the

problem of extreme, suspect contributions to the energy budget estimate.

Date	Regime	Full Budget dT/dt (K/hr)	Budget dT/dt without Vertical Advection (K/hr)	Observed dT/dt (K/hr)
March EET	1	-0.454	-1.706	-1.926
	2	2.690	-1.009	-0.548
March Non-EET	-	150.282	-0.776	0.146
May EET	1	4.252	-2.112	-1.644
	2	-1.699	-9.012	-0.496
May Non-EET	-	9.355	-1.092	-0.644
June EET	1	52.476	3.785	-1.466
	2	27.187	0.352	-0.316
June Non-EET	-	-139.729	11.531	-0.434

Table 6. A comparison of the cooling rate calculated using the full budget, full budget without vertical advection, and the observed cooling rate for each of the case study days. Green cells are cells where the calculated dT/dt more closely matched the observed dT/dt.

When plots are created to examine the behavior of the individual terms across the night,

while neglecting the vertical advection, a better sense can be gleaned of what terms are important

to the formation of the EET. Figure 3-21 follows Figure 3-20, except for the exclusion of vertical

advection. By excluding vertical advection, it is much more easily seen that the radiative flux

divergence, included in the vertical turbulent flux divergence term, is far from the only driver

behind the cooling in the valley. The slopewise advection also contributes largely throughout the

night. The largest observed cooling rate (as seen as the minima in the observed value that occur at

the beginning of the night) corresponds with a large negative cooling rate due to the vertical

turbulent flux divergence. Other dips in the observed cooling rate also correspond to the vertical

turbulent flux divergence, which can be seen in the June EET night in Figure 3-21. This

correspondence holds for each of the EET nights. The slopewise advection, while variable in

time, appears to offset the vertical turbulent flux divergence by providing a warming term during

the rapid cooling of the EET. The horizontal turbulent flux seems also to decrease the cooling rate
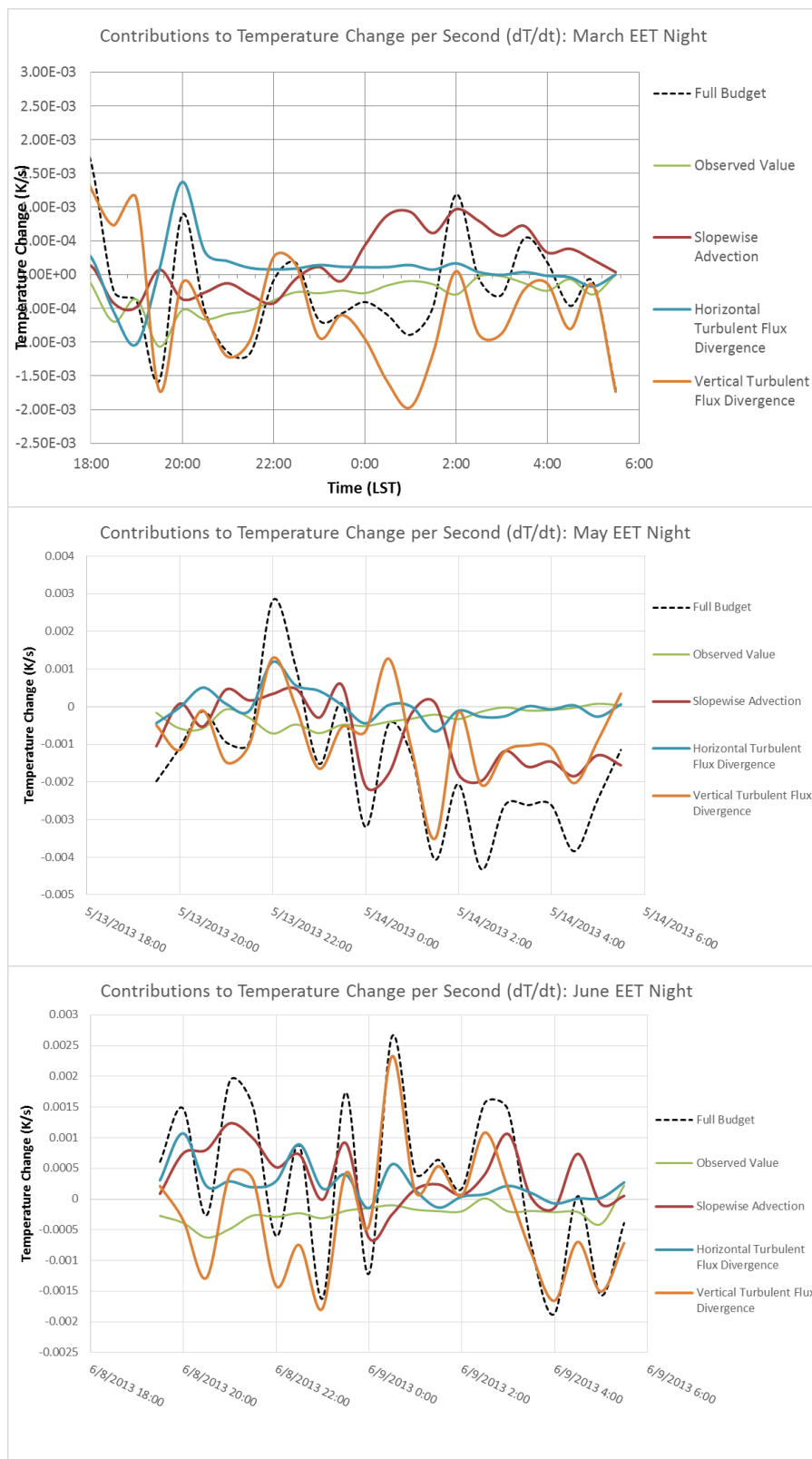
Figure 3-21. Contributions of each part of the surface layer energy budget to the total cooling rate for the EET nights in March, May, and June case studies without the vertical advection term. The full budget is denoted by a dashed line, while the contribution to the full budget from each term is denoted by a solid line. The observed cooling rate is in green.

throughout the 1st regime on EET nights, and appears to reach a constant value approximately at the entrance into the second regime.

The residual, as defined by the difference between the estimated and observed cooling rate, could be explained by the missing advection in the valleywise (u) direction. Since u measurements were taken at the valley bottom station, estimation of the temperature difference required across the valley bottom to fully close the budget is possible. When this was calculated for the case studies (while still neglecting vertical advection), a temperature difference across the valley of only 10^{-2} to 10^{-5} K/m was required. This value is not absurd, so it is possible that budget closure could be accomplished if the network was extended along the valley axis.

When the elements of the surface layer energy budget are plotted for the non-EET nights in each of the case studies, it is fairly simple to see the differences between these nights and the non-EET nights. Figure 3-22 shows the contribution of each term to the overall cooling rate for the non-EET nights in each of the three case studies observed. These nights were generally more turbulent, especially in the vertical. Both turbulent flux terms were larger than those found in the EET case studies, especially the horizontal turbulent flux, which is visible on these plots much more easily than it is on the EET night plots. The advection terms, meanwhile, are still significant but are much closer in magnitude or less in magnitude than those of the turbulent fluxes.
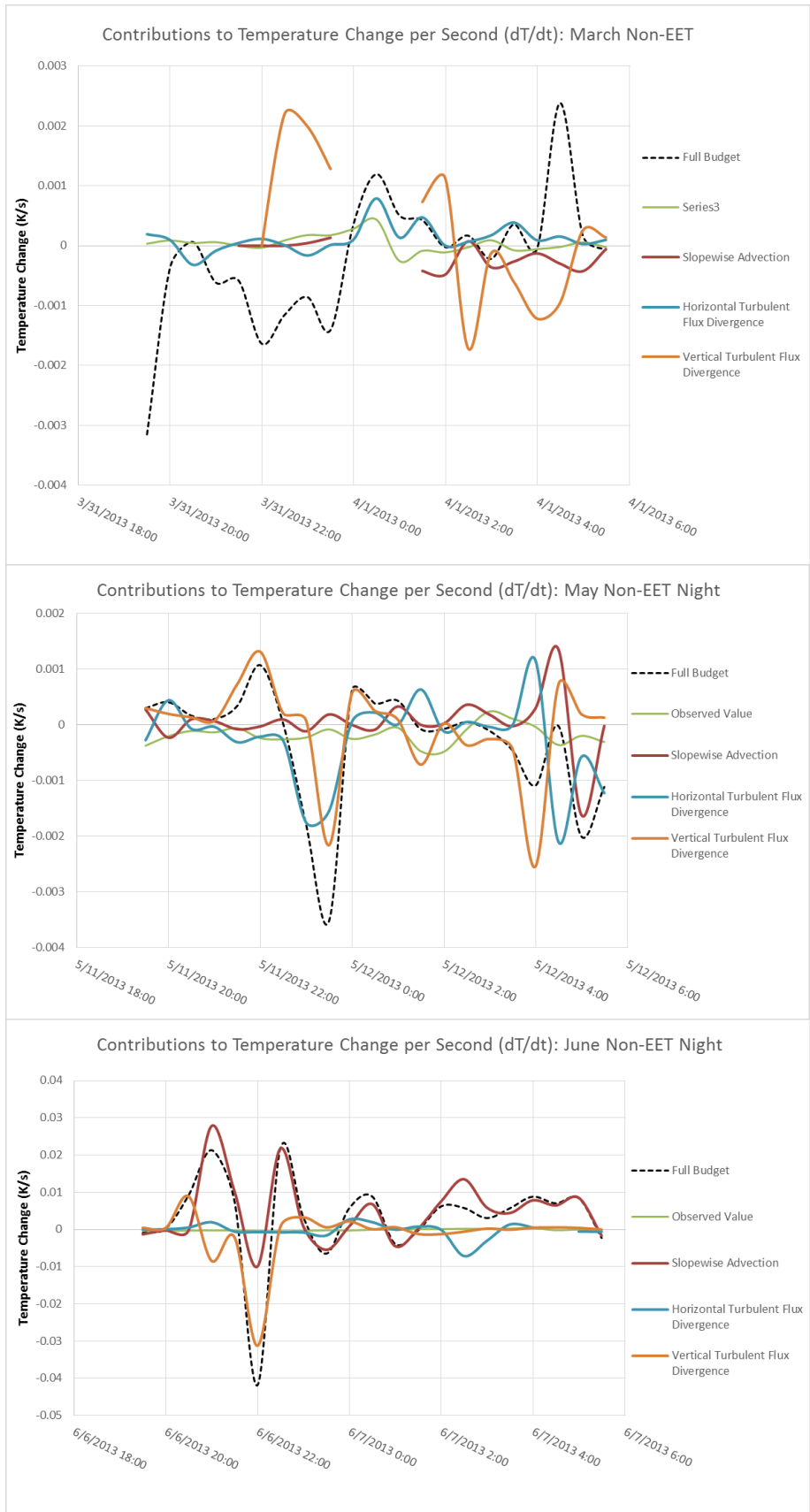
Figure 3-22. Contributions of each part of the surface layer energy budget to the total cooling rate for the non-EET nights in March, May, and June case studies without the vertical advection term. The full budget is denoted by a dashed line, while the contribution to the full budget from each term is denoted by a solid line. The observed cooling rate is in green.

Chapter 4

Conclusions

Nights were able to be classified into two major categories by an analysis of fifteen different variables collected during a three-month study that took place in the Shale Hills Critical Zone Observatory: a small, forested watershed in central Pennsylvania. The eight variables determined to be important in distinguishing the strength of the EET were: date, average net radiation across the night, average tower wind speed, average north slope wind speed, presence of down valley flow, above-canopy wind direction, north slope-valley bottom temperature difference, and tower-valley bottom temperature difference.

The two clusters, formed of EET nights and non-EET nights, differed in average net radiation, average environmental wind speed, the presence or lack of down valley flow, and the stability of the layer between the tower and the valley bottom. Nights that had larger net radiation, calmer winds, the presence of down valley flow, and high stability were the EET nights. Composite temperature fields of both clusters showed a 4K difference in the average total amount of cooling that took place over the night, as well as a difference between the network and the tower at the beginning of the night and the end of the night, suggesting decoupling. There was no evidence of a downslope flow in the middle of each slope in the watershed at .914m, but there was evidence of down valley flow on transition nights at all four sonic anemometers located within the Shale Hills valley, leading to the deduction that down valley flow is occurring in this particular system on EET nights.

A spatial temperature pattern was established within the valley on non-transition nights as well as on transition nights, but the nature of the spatial pattern was much different. A difference in spatial pattern layout within the valley was correlated with the strength of the net radiation, environmental wind speed, and general stability of the atmosphere. The difference is illustrated

by the absolute value of the difference between the two cluster composite temperatures for each sensor. This value shows that a difference in temperature between the clusters is established about midway through the night and then remains stable until early morning. Thus, though a spatial pattern is seen on all nights, the composition of the pattern differs between EET nights and non-EET nights.

The difference in the spatial pattern established across Shale Hills on EET nights and non-EET nights is well-illustrated by a ranking frequency analysis. Non-EET nights had narrower distributions with broader peaks, implying that the spatial pattern and ranking of the sensors that occurs on those nights is extremely consistent. This result is what would be expected if sheltering were a main factor behind the spatial temperature patterns, since the sheltering factors such as vegetation and topography are not mobile and therefore would not change from night to night. However, on transition nights, the distributions were broader. The distributions still demonstrated that if a sensor was cold on one particular transition night, it was likely to be cold on other transition nights as well, but the broadness of the distributions points to the possibility of low-level, subcanopy winds mixing the air and occasionally shuffling the rankings. When the rank evolution throughout the night for EET nights and non-EET nights is examined, the temperature pattern is more clearly illustrated. The non-transition nights show consistent ranking throughout the night, while transition nights show an evolution of individual temperature sensors and differentiation between the slopes.

Fluxes of each pair of case study nights differed mostly between the EET nights and the non-EET nights, rather than between the different months from which the case studies were taken. Spikes in the horizontal, valleywise fluxes whenever a cooling period was begun. These spikes were seen not only in the March and May EET nights, but also in the May non-EET night, whenever a period of EET-like cooling began. Flux magnitudes tended to be larger on EET nights than on non-EET nights as well, and the vertical fluxes tended to be in opposite directions toward

the end of the evening on EET nights vs. non-EET nights. Momentum fluxes calculated using the vertical and valleywise wind perturbations also tended to switch signs at all stations as the night wore on in the EET cases, providing further indication that downvalley flow was prevalent on EET nights.

When the energy budgets were calculated, the vertical advection term dominated the other terms in the surface layer energy budget. This domination led to wholly unreasonable estimated cooling rates up to an order of magnitude larger than the observed cooling rate at the bottom of the night. Neglecting the vertical advection and the dividing the EET night into two regimes – one with rapid cooling, and another with steady, slower cooling – allowed for more insight into the dominant terms in estimating the cooling rate at the bottom of the valley. Determining the cooling rate at the bottom of the valley is an important first step that could be extrapolated to the rest of the valley with a greater extent of sonic anemometer deployment.

Net radiation divided by a characteristic depth was found to not be enough to explain the observed cooling rate in the valley, particularly during the rapid cooling of the first regime on EET nights. In fact, the net radiation had the largest magnitude at the end of the night, when the cooling rates tended to be smallest. The slopewise advection, as well as the vertical turbulent flux divergence, had leading-order effects on the final cooling rate estimate. Thus, treating the trunk space of the canopy as isothermal and non-turbulent overlooks important mechanisms to the formation of spatial temperature patterns within the canopy and complete dynamical systems. When the difference between the calculated cooling rate without vertical advection and the observed cooling rate was treated as a residual, the dT/dx in the valleywise direction was on the order of 10^{-2} to 10^{-5} K/m, which is not unreasonable. These measurements capture many important terms to the cooling rate at the bottom of the network, particularly during the rapid cooling regime of EET nights, but the resolution in the measurements prevents a deterministic solution to the energy budget. The non-EET nights were found to differ from the EET nights in the

importance of terms, with the turbulent flux terms playing a larger role with regards to the overall cooling rate in the non-EET nights, and the advective terms taking a lesser role. Radiation was also much less influential on non-EET nights than on EET nights.

Acevedo and Fitzjarrald's (2001) work classified the EET based on a temperature decrease, a decrease in surface wind speed and a jump in the specific humidity. Greater variation in these variables after sunset relative to the rest of the night was the inspiration for their EET. However, this study has uncovered several other characteristics of EET nights as compared to non-EET nights.

EET nights differ from non-EET nights in many basic state variables. The total amount of cooling in the valley relative to the tower top is one such difference. EET nights in this study had temperature differences of 4-5K between the 30m tower and the valley bottom. Non-EET nights had differences of only 3-4K, which is still a large difference. Net radiation was found to be very different on EET nights as compared to non-EET nights as well, with a difference of $20W/m^2$ between the two nights. Since the average net radiation across each of these nights was on the order of tens of W/m^2, this difference is highly significant. The winds above-canopy are much calmer on EET nights than non-EET nights, with average wind speeds rapidly decreasing during the first half of the night from 3m/s to ~1m/s and remaining around 1m/s for the remainder of the night. This contrasts with the constant ~2m/s wind seen on non-EET nights.

The persistent spatial temperature patterns revealed by the ranking analysis evolved very differently during the EET period, as can be seen from the cluster temperature difference. However, once the EET period was complete, the patterns evolved in similar manners. The ranking analysis also showed that the slopes of the valley differed in temperature from one another on EET nights. The north slope had cooler rankings, while the south slope maintained warmer rankings. This differential only happened on EET nights and evolved throughout the EET period. Once the EET was over, these rankings remained relatively steady.

Two temperature regimes were seen on EET nights. The first regime included the period of rapid cooling during the EET, while the second regime encompassed the steady cooling that occurred once a spatial pattern in temperature across the network had been established. No clear link between the change in regimes and environmental characteristics of the EET was able to be found in this study. Though drainage flows are observed at the sonic anemometers, the shift in wind direction on the slopes occurs very early in the night, at the start of the EET. The change in regimes does not occur until the end of the EET. The net radiation decreases steadily throughout the night, and an increase in the depth over which the radiative flux divergence is acting could cause the change in the regimes.

Cold pools located at the Shale Hills Critical Observatory are unable to be confirmed on either EET nights or non-EET nights. While the valley bottom sensor is often the coldest sensor on EET nights, it was occasionally the warmest sensor as well. Shale Hills is not an enclosed valley or a sinkhole. It has an outlet, and so cold air that drains to the bottom of the valley would be able to drain out through the valley outlet. Several large, low-lying geographic features surround Shale Hills (such as the drained Lake Perez) that the cold air could be funneled into.

Acevedo and Fitzjarrald (2001) worked with a range of valleys, placing their sensors at varying elevations within the valleys. The conclusions they reached were based on several different valleys. This study has shown that the temperature patterns they observed on a larger scale can also be observed on a smaller, single-valley scale at different elevations within the valley. It has then gone on to characterize environmental conditions related to the EET both within the valley and at a larger scale.

With these findings, new light is shed on the importance of below-canopy measurements during both leaf-off and leaf-on time periods. Unlike what is suggested by or assumed by much of the literature on vegetated areas, the horizontal trunk space of this network was found to be far from isothermal during both the leaf-on and leaf-off periods of the night, and even the vertical

trunk space was not isothermal. In temperature or potential temperature, a spatial temperature pattern occurred within the valley, on the orders of tens of meters.

Further studies could go beyond characterization of the EET and explore the timing of regime shift with regards to environmental characteristics. While the terms in the surface layer energy balance were quite noisy (with the exception of radiation), these terms could be refined and analyzed to provide better estimation of the cooling rate. Refined terms could also be examined with regards to the timing of the regime shift, to determine if one term or a combination of terms is responsible for the shift. Further work could also break down the valley into the two slopes and attempt to calculate an energy budget for each slope; these budgets could then be compared to the rate of change of the temperature sensor found in the middle of each slope.

Appendix A

Temperature Traces for Case Study Comparisons

March EET Case Study Network Temperatures

March Non-EET Case Study Network Temperatures

May EET Case Study Temperatures

May Non-EET Case Study Temperatures

June EET Case Study Temperatures

June Non-EET Case Study Network Temperatures
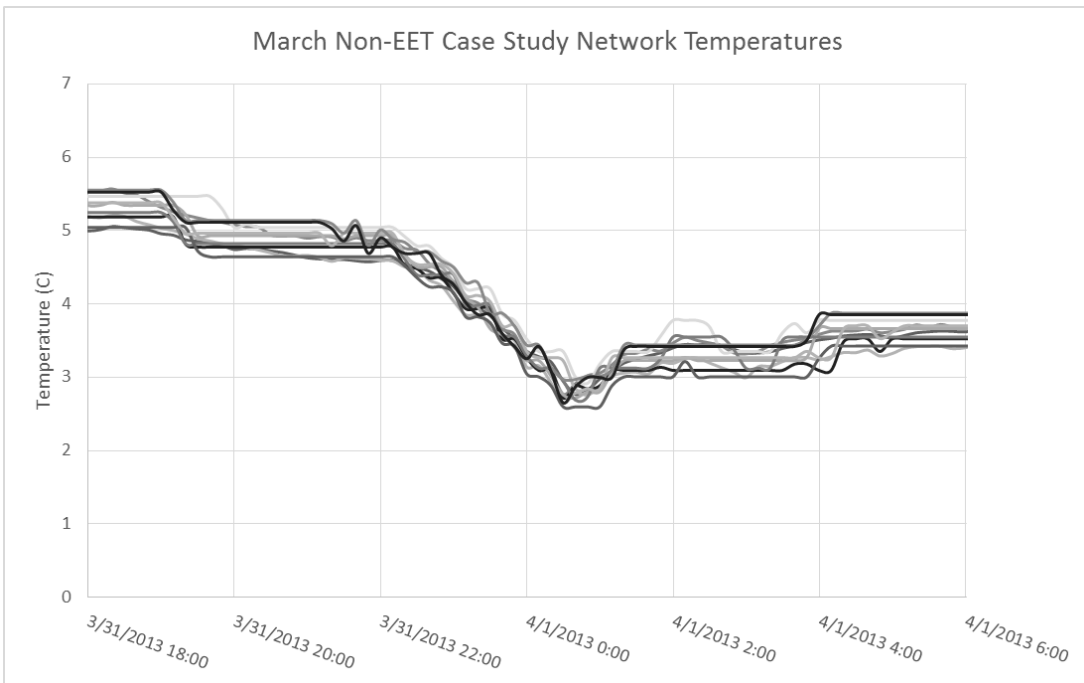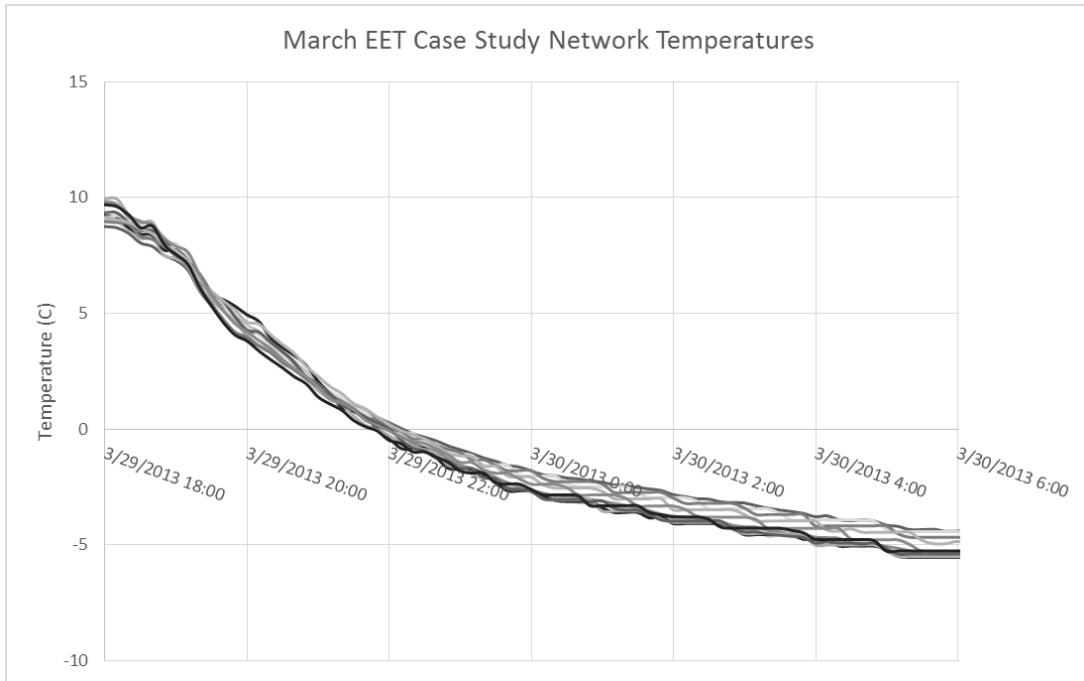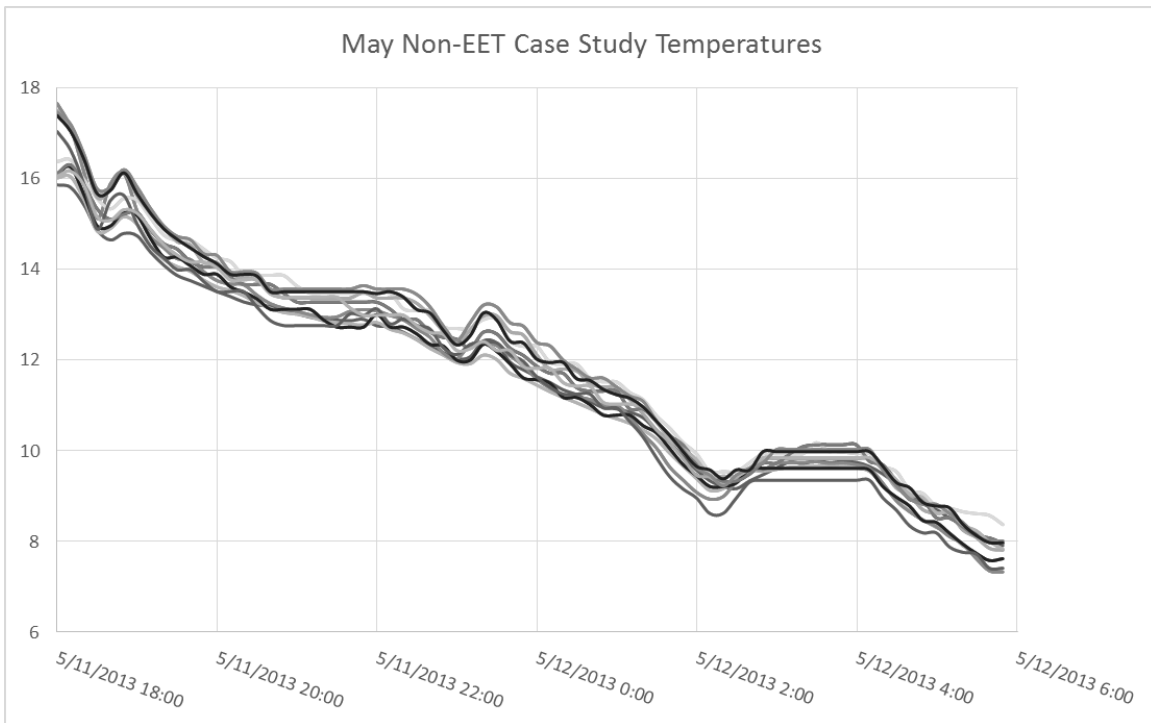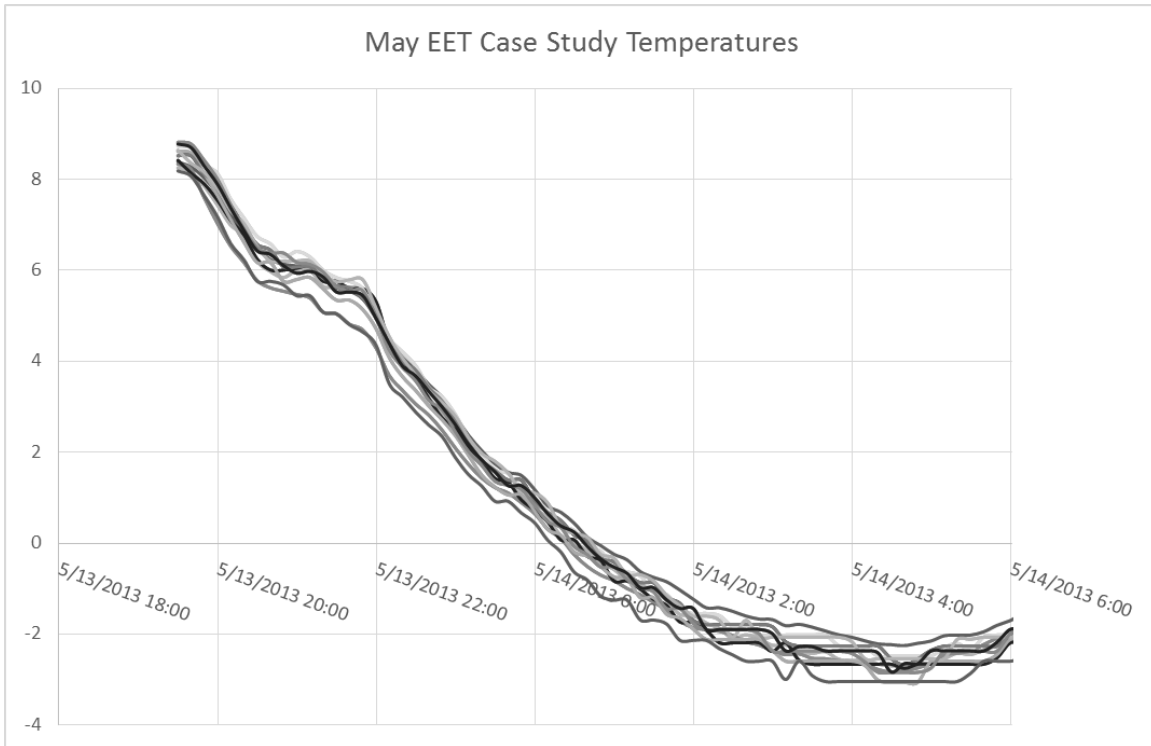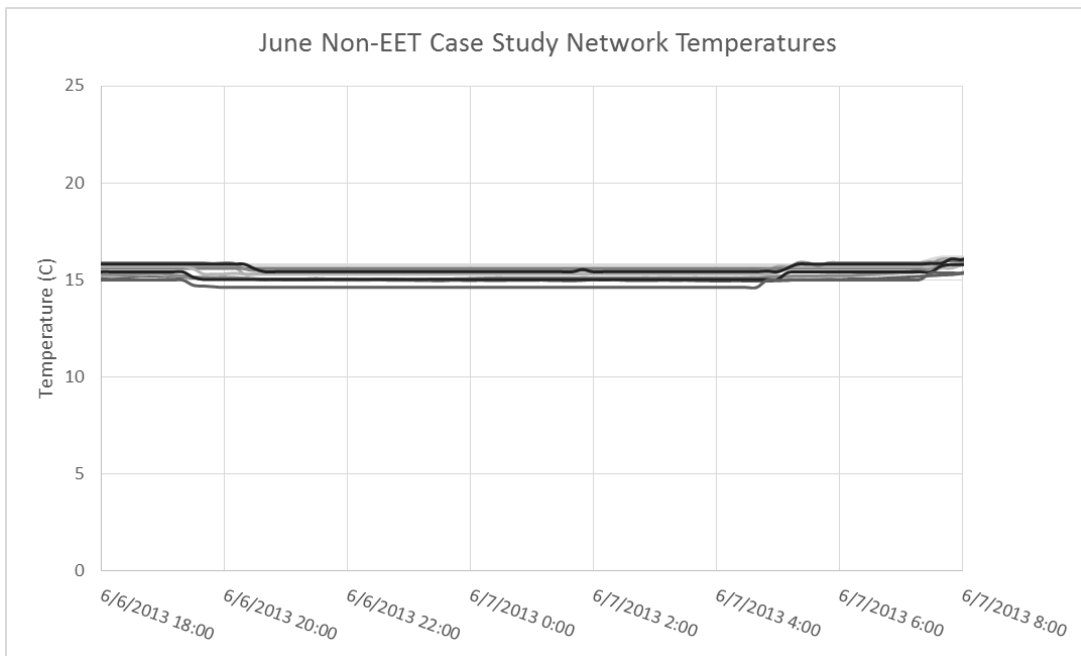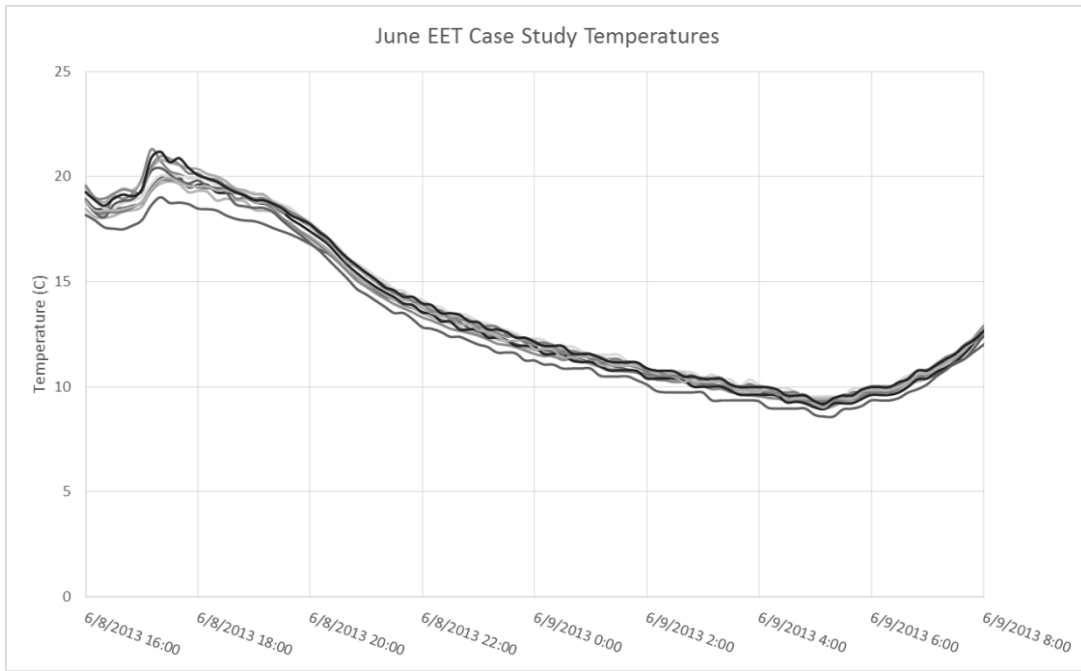
REFERENCES

Acevedo, O.C., and D.R. Fitzjarrald. 2001. The early evening surface-layer transition: temporal and spatial variability. *J. Atmos. Sci*. **58**, 2650-2667.

Baldocchi, D., and T.P. Meyers. 1987. Turbulence structure in a deciduous forest. *Boundary-Layer Meteorol*. **43**, 345-364.

Barry, R.G. 2008. Mountain Weather and Climate, 3ʳᵈ Edition.

Belcher, S.E., J.J. Finnigan, and I.N. Harman. 2008. Flows through forest canopies in complex terrain. *Ecol. Appl*. **18**, 1436-1453.

Bodine, D., P.M. Klein, S.C. Arms, and A. Shapiro. 2009. Variability of surface air temperature over gently sloped terrain. *J. Appl. Meteorol. Clim*. **48**, 1117-1141.

Boldes, U., A. Scarabino, and J. Coleman. 2007. About the three-dimensional behavior of the flow within a forest under unstable conditions. *J. Wind. Eng. Ind. Aerod*. **95**, 91-112.

Chen, H., and C. Yi. 2012. Notes and correspondence: Optimal control of katabatic flows within canopies. *Q. J. R. Meteorol. Soc*.

Christen, A., E. van Gorsel, R. Vogt, M. Andretta and M.W. Rotach. 2001. Ultrasonic anemometer instrumentation at steep slopes wind tunnel study – field intercomparison – measurements. *MAP Newsletter*. **15**, 164-167.

Finnigan, J. 2000. Turbulence in plant canopies. *Annu. Rev. Fluid. Mech*. **32,** 519-571.

Fleagle, R.G. 1950. A theory of air drainage. *J. Meteorol*., **7,** 227-232.

Froelich, N.J., C.S.B. Grimmond, and H.P. Schmid. 2011. Nocturnal cooling below a forest canopy: Model and evaluation. *Agric. For. Meteorol*. **151**, 957-968.

Gustavsson, T., M. Karlsson, J. Bogren, and S. Lindqvist. 1998. Development of temperature patterns during clear nights. *J. Appl. Meteorol*. **37**, 559-571.

Gustavsson, T. 1995. A study of air and road-surface temperature variations during clear windy nights. *Int. J. Climatol*. **15**, 919-932.

Haiden, T. and C.D. Whiteman. 2005. Katabatic flow mechanisms on a low-angle slope. *J. App. Met.* **44**, 113-126.

Hall, M., E. Frank, G. Holmes, B. Pfahringer, P. Reutemann, and I.H. Witten. 2009. The WEKA Data Mining Software: An Update. *SIGKDD Explorations* **11**, Issue 1.

Hammerle, A., A. Haslwanter, M. Schmitt, M. Bahn, U. Tappeiner, A. Cernusca, and G. Wohlfahrt. 2007. Eddy covariance measurements of carbon dioxide, latent and sensible energy fluxes above a meadow on a mountain slope. *Boundary-Layer Meteorol*. **122**, 397-416.

Helmis, C.G., and K.H. Papadopoulos. 1996. Some aspects of the variation with time of katabatic flow over a simple slope. *Q. J. R. Meteorol. Soc*. **122**, 595-610.

Karlsson, I.M. 2000. Nocturnal air temperature variations between forest and open areas. *J. Appl. Meteorol*. **39**, 851-862.

Laughlin, G.P., and J.D. Kalma. 1990. Frost risk mapping for landscape planning: a methodology. *Theor. Appl. Climatol*. **42**, 41-51.

Lundquist, J.D. and D.R. Cayan. 2007. Surface temperature patterns in complex terrain: daily variations and long-term change in the central Sierra Nevada, California. *J. Geophys. Res*. **112**, D11124.

Mahrt, L., D. Vickers, R. Nakamura, M.R. Soler, J. Sun, S. Burns, and D.H. Lenschow. 2001. Shallow drainage flows. *Boundary-Layer Meteorol*. **101**, 243-260.

Mahrt, L. 1982. Momentum balance of gravity flows. *J. Atmos. Sci.* **39**, 2701-2711.

Manins, P.C. 1992. Vertical Fluxes in Katabatic Flows. *Boundary-Layer Meteorol.* **60**, 169-178.

Sedlák, P., M. Aubinet, B. Heinesch, D. Janous, M. Pavelka, K. Potuzníková, and M. Yernaux. 2010. Night-time airflow in a forest canopy near a mountain crest. *Agric. For. Meteorol*. **150**, 736-744.

Shapiro, A., P.M. Klein, S.C. Arms, D. Bodine, and M. Carney. 2009. The Lake Thunderbird micronet project. *B. Am. Meteorol. Soc*. **90**, 811-823.

Shaw, P.H., K.T. Paw U, X.J. Zhang, W. Gao, G. Den Hartog and H.H. Neumann. 1990. Retrieval of turbulent pressure fluctuations at the ground surface beneath a forest. *Boundary-Layer Meteorol*. **50**, 319-338.

Staebler, R.M., and D.R. Fitzjarrald. 2005. Measuring canopy structure and the kinematics of subcanopy flows in two forests. *J. Appl. Meteorol*. **44**, 1161-1179.

Stull, R.B. 1988. *An Introduction to Boundary Layer Meteorology*. Dordrecht: Kluwer Academic.

Tabony, R.C. 1985. Relations between minimum temperature and topography in Great Britain. *J. Climatol*. **5**, 503-520.

Tang, Z., and J. Fang. 2006. Temperature variation along the northern and southern slopes of Mt. Taibai, China. *Agric. For. Meteorol*. **139**, 200-207.

Tóta, J., D.R. Fitzjarrald, and M. A. F. da Silva Dias. 2012. Amazon Rainforest exchange of carbon and subcanopy air flow: Manaus LBA site – a complex terrain condition. *Sci. Wor. J.* **2012**, 1-19.

Turnipseed, A. A., D. E. Anderson, P.D. Blanken, W.M. Baugh and R.K. Monson. 2003. Airflows and turbulent flux measurements in mountainous terrain Part 1. Canopy and local effects. *Agric. For. Meteorol*. **119**, 1-21.

Vergeiner, I., and E. Dreiseitl. 1987. Valley winds and slope winds – observations and elementary thoughts. *Meteorol. Atmos. Phys*. **36**, 264-286.

Vosper, S.B., and A.R. Brown. 2008. Numerical simulations of sheltering in valleys: the formation of nighttime cold-air pools. *Boundary-Layer Meteorol*. **127**, 429-448.